

THESIS

ADVANCED PHOTOVOLTAIC MODULE ARCHITECTURE FOR HIGH VALUE RECYCLING
AND LOWER COST

Submitted by

Ryan J.E. Ruhle

Department of Mechanical Engineering

In partial fulfillment of the requirements

For the Degree of Master of Science

Colorado State University

Fort Collins, Colorado

Fall 2023

Master's Committee:

Advisor: Walajabad Sampath

James Sites

Christopher Weinberger

Copyright by Ryan J.E. Ruhle 2023

All Rights Reserved

ABSTRACT

ADVANCED PHOTOVOLTAIC MODULE ARCHITECTURE FOR HIGH VALUE RECYCLING AND LOWER COST

As climate concerns continue to bolster solar energy production, the need to consider how solar panels are treated at end of life as well as the cost of solar panel production is becoming a more significant issue. Traditionally, Crystalline Silicon (c-Si) solar panels are made by laminating solar cells with glass under high heat and high mechanical pressure. The most common material used for this lamination between the glass and the c-Si solar cell is Ethylene Vinyl Acetate (EVA), a copolymer of ethylene and vinyl acetate. The first and primary issue is that it requires high temperature and a significant amount of pressure to be adhered to both the glass and the c-Si cell. Another related issue is that the c-Si cell and EVA encapsulant do not have the same thermal expansion coefficients. This leads to stresses which can cause the formation and growth of microcracks which can hinder performance and reliability of the effected solar cells. End-of-life recycling is also significantly hampered by cross-linking of EVA.

The Materials Engineering Laboratory (MEL) has long worked on vacuum lamination free module architectures, though this has been primarily for use for Cadmium Telluride (CdTe) solar panels. These CdTe panels have passed IEC 61215 tests and have been applied in the field. These Edge-sealed photovoltaics modules based on Insulating Glass (IG) industry technology have many advantages including lower cost, improved manufacturability, increased durability, and enable high-value recycling with the potential for material reuse. The edge-sealed modules eliminate EVA (Ethylene Vinyl Acetate) lamination, but a gap filled with air or inert gas between the glass and solar cell increases optical reflection losses. The use of edge sealed modules for c-Si was explored in this study. A prototype manufacturing system (2 ft X 4 ft substrates) has been developed at MEL and was used in this study.

Many c-Si modules were fabricated with edge sealing and were studied at the National Renewable Energy Laboratory (NREL) in various tests including accelerated tests. These studies have shown that optical reflection losses can be reduced by using nanostructures made from acrylic polymers. The nanostructures are produced by hot embossing which is intrinsically a low-cost process. The edge sealed structure has demonstrated extreme robustness to moisture ingress (5000 hrs. vs 1000 hrs. in damp heat), improved mechanical robustness, significant reduction in Potential Induced Degradation (PID), survive thermal cycling and small manufacturing footprint (80% less) while improving module reliability. The edge sealed modules have demonstrated high value recycling of the components and have the potential to make recycling of c-Si PV modules economical.

ACKNOWLEDGEMENTS

First, I would like to acknowledge my committee for the significant time and effort to make this a possibility. Thank you for your input, advice, and suggestions. To Dr. Sites for introducing me to the PV lab when I was an undergraduate physics student. To Dr. Weinberger for being so complete on your course instruction. To Dr. Sampath, for all of the help with the encapsulation project here. Dr. Sampath has trusted me to work independently and make a great many choices without a significant amount of oversight, all while making himself available when I needed help. I recognize that he has entrusted me with a great many things related to the lab.

I'd like to also thank my mother and my grandparents, who were responsible for raising me. My mother graduated from law school at the age of 45 and has been an inspiration for me returning to college as well. When I was 16, I blew the engine on my first car. My grandfather helped me pick out a new engine and purchased a repair manual and left me to my own devices in a dirt parking space on his land until the car once again ran. This has been a particularly big inspiration for me getting into mechanical engineering and helped ignite my passion for wanting to understand the way things worked.

I would like to thank my collaborators at NREL, Steve Johnston and Dana Kern, for working with me to test and monitor the samples that were made. For also providing samples for direct comparison and ensuring that samples were getting through tests that needed to be done. This has been an invaluable resource and I look forward to continuing my collaboration with them and their team. And of course, Kent Terwilliger, for being a fantastic technician and always providing up-to-date information on the status of various tests and ensuring the equipment and testing machines were always functioning properly.

To Dr. Richard Eykholt, who pushed me probably harder than any professor ever has. While it certainly meant a few sleepless nights and an over-consumption of caffeine, I will never forget that when I had made it through it all, you reminded me that "Now you know nothing can stop you". To the men

and women I served with, and those veterans who I have worked with, thank you for your brother and sisterhood. Nothing makes me prouder to have accomplished so much with my GI bill and to be able to stand proud and say that our service meant not just sacrifice, but valuable skills which cannot be taught, but only forged in the most intense of crucibles.

To my team and fellow students at the PV manufacturing lab I've worked with along the way, thank you for all of your help, hard work, and support in getting here. David and Larry, I could not possibly ask for a better crew with which to accomplish things. You are always on top of things and full of great ideas, but also willing to work and get the job done. To Marc, you've been invaluable in fabricating all of the intricate parts necessary to fabricate samples and work towards the future. To Lilly, thank you for all of the reflection data, which I know I asked to have experiments repeated more than once until I was confident everything was done correctly. To Camden, thank you for providing the invaluable irradiance of our own laboratories Xenon lamp, which was absolutely key in getting results.

I would not be here without the help of so many instructors, family, collaborators, team members, fellow members of the armed services, and fellow students. To everyone who made all of this possible, thank you.

AUTOBIOGRAPHY

Ryan Ruhle is currently a graduate student at Colorado State University in the Mechanical Engineering Department. After struggling to find funds to complete his undergraduate degree, he joined the U.S. Military as a Cavalry Scout in the Army. This not only gave him access to the GI bill, but also provided him with a significant amount of experience in terms of problem solving and collaboration.

TABLE OF CONTENTS

ABSTRACT ii

ACKNOWLEDGEMENTS iv

AUTOBIOGRAPHY vi

LIST OF TABLES ix

LIST OF FIGURES x

Chapter 1: INTRODUCTION 1

 1.1 Introduction to the Technology..... 1

 1.2 Climate Change and the Growing PV Industry:..... 4

 1.3 Hypotheses Identified and Research 7

 1.3.1 Hypothesis 1:..... 7

 1.3.2 Hypothesis 2:..... 9

 1.3.3 Hypothesis 3:..... 10

 1.3.4 Hypothesis 4:..... 11

Chapter 2: LITERATURE REVIEW..... 12

 2.1 Introduction 12

 2.2 Previous Adaptations for c-Si 13

 2.3 Optical Analysis 15

 2.4 Mechanical Advantages 17

 2.5 Moisture Ingress Modeling 17

 2.6 Recent Publications..... 19

Chapter 3: EXPERIMENTAL DESIGN..... 23

 3.1 Introduction 23

 3.2 Equipment and Sample Manufacturing 23

 3.2.1 MEL’s Manufacturing Equipment: 24

 3.3.2 Sample Fabrication..... 26

 3.3.3 Testing and Measurement Equipment Used:..... 28

 3.3 Hypothesis 1..... 32

 3.4 Hypothesis 2..... 33

 3.5 Hypothesis 3..... 35

 3.6 Hypothesis 4..... 35

Chapter 4: RESULTS AND DISCUSSION 43

4.1 Introduction	43
4.2 Hypothesis 1.....	43
4.3 Hypothesis 2.....	45
4.4 Hypothesis 3.....	46
4.5 Hypothesis 4.....	49
Chapter 5: CONCLUSIONS	51
5.1 Conclusions	51
5.2 Future work and recommendations	53
REFERENCES.....	55
APPENDIX A- PUBLICATIONS	57

LIST OF TABLES

Table 1: This table should have a description. 30

Table 2: Significant results from samples tested in DH conditions. Samples are removed from DH testing chamber every 1,000 hours and the moisture indicators are observed..... 44

Table 3: Time for each process step 45

Table 4: Table is a placeholder. Will go over statistical significance factors/indicators tabulated results. Have data, will make pretty. discussion. 48

LIST OF FIGURES

Figure 1: Image depicting the difference between traditionally manufactured c-Si modules (left) versus ESM technology developed at MEL (right).....	2
Figure 2: Layered reflectance model comparison between ESM (left) and traditional modules (right). Model uses $T = 1 - R$. Texture is modeled based on manufacturer data. Reflectance data for glass and cell are integrated numerically over AM 1.5 using data from MEL. Model suggests that power between modules should be similar.	3
Figure 3: Data available at climate.nasa.gov of the global temperature anomaly since prior to the industrial revolution.....	5
Figure 4: Yearly increase in cumulative global installations of PV and Wind since 2000 provided by NREL.	6
Figure 5: Traditional module wiring scheme (left) versus ESM wiring scheme (left). The wires in the ESM wiring scheme are brought through the edge of the module between the layer of PIB and silicone is injected around the edge of the wires.....	7
Figure 6: High-value recycling process steps for module disassembly with components completely separated.	9
Figure 7: Electroluminescence (EL) image of ESM Module (left) no microcracks formed during encapsulation. Traditional glass-glass module (right) with formation of microcracks.	10
Figure 8: Schematic comparison of the standard module architecture (top) and NICE module technology (bottom) (Dupuis, 2009).	13
Figure 9: Spectral emission of typical unfiltered Xenon lamp compared directly to AM1.5G as a function of wavelength [Couderc, 2017].	15
Figure 10: Comparison of various degradation mechanisms experienced by solar modules between traditional lamination modules and CSU's ESM module architecture.	20
Figure 11: Depiction of progress improvements in matching power to traditional modules. 100% is a 1-1 match for idealized power.....	21
Figure 12: Graco supplied heated PIB pumping system (left) and polymer application tooling shown with 30cm x 30cm adapter plate installed (right).	24
Figure 13: Image of pneumatic press utilized at MEL.	25
Figure 14: Tool hardware configuration.	25
Figure 15: Sample fabricated by MEL for the purpose of accelerated longevity testing at NREL.....	26
Figure 16: A3 testing chamber configuration. Test conditions are described in table 1.....	29
Figure 17: EL and PL measurement device in PL configuration. Each of the adjustable black arms are designed to emit a laser which is above the bandgap. This excites electrons and generates luminescence directly from the sample.....	30
Figure 18: Xenon IV testing equipment available at NREL without Xenon solar simulator illuminated.	32
Figure 19: Three samples for testing as prepared. Top- no busbar ribbons or desiccant carrier. Bottom left- Busbar ribbons and desiccant carrier on interior of module. Right- Busbar ribbons and no desiccant carrier. Note that the leads are held in place as was learned during process optimization.	32
Figure 20: Sample optimization for process conditions taking place iteratively as best practices is established to create uniformity in production and best possible sample. An Approximate 8.5% relative reduction in performance in I_{sc} is noted when testing under LED lamp conditions measured by NREL. ...	37

Figure 21: Experimental setup for testing tiny modules which are similar to traditional encapsulation (left) and MEL’s module architecture. This design is not the full finalized design, but rather small cells which can fit in the available testing apparatus at the MEL. 38

Figure 22: Measured reflection losses as a function of wavelength and adjusted to AM 1.5 incidence. Note that most of the gains are within the visible spectrum (380-700nm) especially when applied to the c-Si cell. 39

Figure 23: QE data as a function of wavelength normalized to number of incident photons courtesy of collaboration with NREL. Data is corrected for reflectance such that photons incident to the cell itself are considered..... 41

Figure 24: Glass-glass EVA module fabricated at NREL for comparison. Post-encapsulation (left) shows degradation due to extreme process conditions while post accelerated stress (right) demonstrates how microcracking can grow during stress tests. 47

Figure 25: EL image pre and post processing utilizing Sobel edge detection methods. While the wires show up as not illuminating, it is more important to ask whether or not this grows. The circled image in the right shows the detection of an imperfection in the cell, however, it is not observed to have grown during accelerated stress testing. 47

Figure 26: 20cm x 30cm 6 cell 20-watt prototype module fabricated at MEL. This is the most recent and most powerful module created by the multitude of processes developed at MEL for c-Si to date. Cells are of a configuration which is also extremely resilient against UV degradation. 52

Chapter 1: INTRODUCTION

1.1 Introduction to the Technology

Photovoltaics (PV) is the process of converting sunlight directly into electricity. Solar cells are the primary means by which this process is accomplished, and these are made from materials known as semi-conductors. Radiated light incident on the solar cell excites an electron from the valence band to the conduction band across what is called a bandgap. This generates an electron hole pair which can drive a current based on principles found in condensed matter physics. There are several different types of semi-conductors which are currently being researched, however, the most popular type of solar cell used to generate electricity is crystalline silicon or c-Si. This type of solar cell accounts for around 93% of the global production of solar cells and will be the primary focus of the research discussed here (Green, 2016). Single-crystal c-Si cells are manufactured in abundance globally and have been the most thoroughly developed. Due to this, the cost of PV electricity generation has reached new lows and is steadily becoming an important source of power generation for the globe.

C-Si solar cells still face challenges in the manufacturing process and further reduction of costs as well as end-of-life treatment of solar cells and the panels in which they reside is still a rapidly growing field of research. The architecture of the panel or module, mechanical properties, lifespan, and processes involved are still being advanced (Handara, 2017). The traditional architecture and process is still not yet perfected and has been shown to have observable flaws which shorten the lifespan of PV products and reduce the ability to recover valuable materials used in manufacturing at the end-of-life. One of the major issues relates to the process conditions which traditional modules are manufactured under. This is because typical solar cells are vacuum laminated under process conditions which reach up to 200C and are pressed together. Since there are varying rates of thermal expansion for the solar cell

and the material (typically EVA) which the cell is encapsulated in, as well as high pressures which can exist on the thin wires which conduct electricity, this process is known to damage solar cells. It has also been shown that through thermal cycling which occurs naturally during the lifespan, these solar cells can develop microcracks early in their lifespan and those cracks are able to grow throughout the module life in a process known as microcrack growth and formation. This process is also costly in terms of manufacturing equipment, material use, and includes a lengthy process time (Tushar, 2019). In order to avoid these issues and reduce manufacturing and material cost, it is proposed that the entire vacuum lamination process and encapsulant can be replaced with an air gap or potentially inert gas which has been shown to reduce the encapsulation process by 2 cents per watt peak in both material cost and manufacturing equipment cost (Barth, 2018). The module novel module architecture which is proposed in this thesis eliminates the costly vacuum lamination process and simplifies the overall manufacturing process. This type of module will be referred to as an Edge Sealed Module (ESM). depiction of the differences between traditionally manufactured modules compared to the ESM is shown in figure 1.

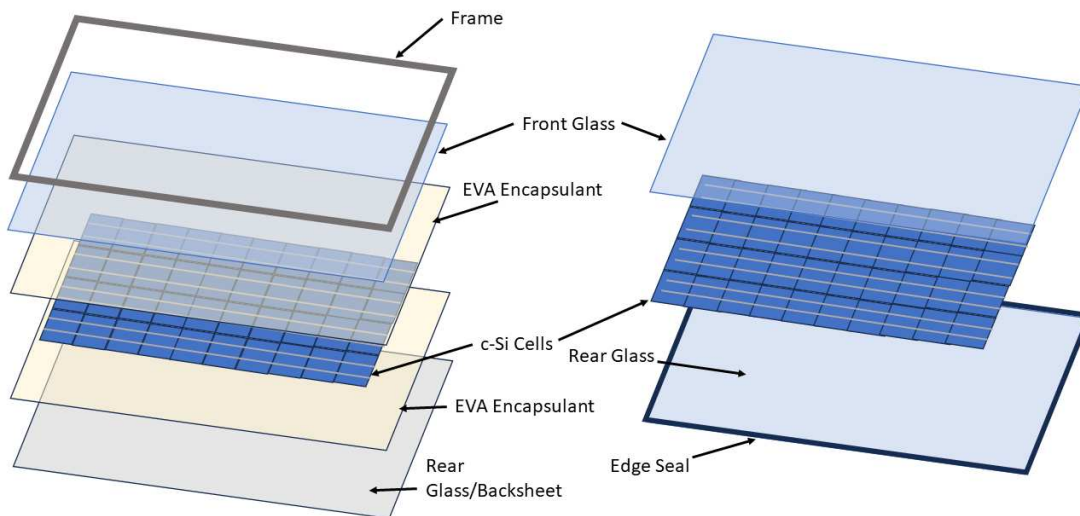


Figure 1: Image depicting the difference between traditionally manufactured c-Si modules (left) versus ESM technology developed at MEL (right).

However, this idea introduces its own issues which must be addressed for c-Si modules. This is because the EVA serves the purpose of light coupling from the glass to the solar cell. This is due to Fresnel's equations of reflectivity. At a most basic level, glass has a refractive index of 1.5 and air or inert gas has an index of refraction of 1.0, while the cell itself has an index of refraction of around 2.2. Comparatively, EVA has an index of refraction nearly equal to glass. In the simple case of direct light, the reflectance where two mediums meet can be written as:

$$R = \left| \frac{n_1 - n_2}{n_1 + n_2} \right|^2 \quad (1)$$

Where R is the reflectance, n_1 is the index of refraction of the first medium, and n_2 is the index of refraction of the second medium. This becomes somewhat problematic the further apart two indices of refraction become. Without the EVA, the air gap introduced increases the difference between the indices of refraction of the varying layers by quite an amount which in turn generates significant reflectance losses due to lack of incident light on the solar cell.

If there is too much reduction in performance, having a more reliable and lower cost PV module no longer is financially reasonable as the cost of panels decreases while the cost of land is increases

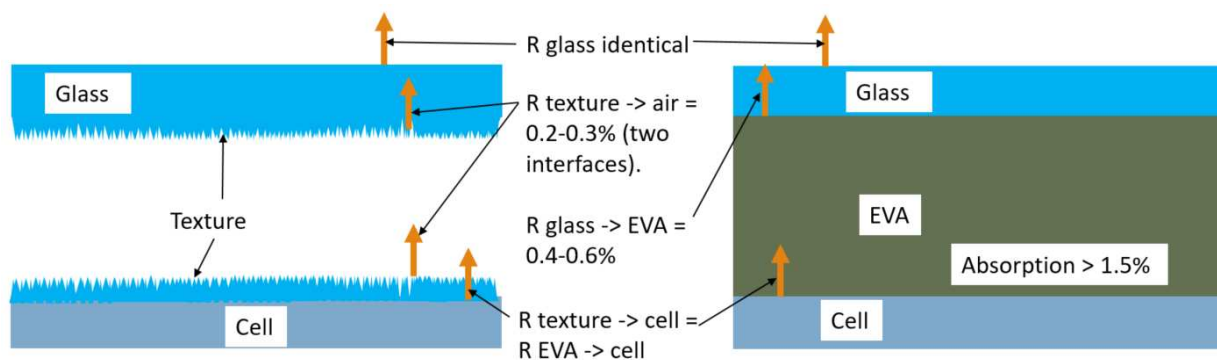


Figure 2: Layered reflectance model comparison between ESM (left) and traditional modules (right). Model uses $T = 1 - R$. Texture is modeled based on manufacturer data. Reflectance data for glass and cell are integrated numerically over AM 1.5 using data from MEL. Model suggests that power between modules should be similar.

(Wiser, 2020). Researchers at MEL have been working on a potential solution to this issue in order to improve the performance of PV modules which have a gas or air gap which utilizes an internal texture. This technology is currently under provisional patent with development and testing of this is continuing at MEL. With an internal texture, light is still reflected, however, rather than being reflected directly back into space, incident light which is reflected is instead re-directed into the module to have another chance at being absorbed and converted to electricity. A cross-section of the ESM optical design compared to traditional vacuum laminated modules can be found in figure 2.

These values are based on manufacturer data which was obtained on data sheets provided publicly by the respective manufacturers. Precise by wavelength data is measured experimentally by MEL in section 3.6 during the experimental section.

1.2 Climate Change and the Growing PV Industry:

Climate change refers to the increase in global average temperature in response to increased greenhouse gases in the atmosphere such as CO₂. The industrialized world has relied on energy sources such as coal and natural gas in order to produce electricity, which has been an important factor in global modernization. However, this has not come without consequence. Rising CO₂ levels, which have recently reached in the region of 420 parts per million (ppm) has led to a steady increase in average global temperatures. This has created a temperature anomaly of 1 degree Celsius since the time of industrialization and is continuing an ever upward trend. The problem is not simply that the average temperature has risen slightly, but rather that the individual climates of the Earth are in a chaotic system. Due to the chaotic nature of the Earth's climates, this means that localized effects are much larger than the overall input to the system. Areas which are generally productive for agriculture may experience rapid shifts which can in turn lead to food scarcity which disproportionately impacts impoverished communities. According to data which can be found at climate.nasa.gov, arctic sea ice has declined

12.6% per decade, 151 billion metric tons of ice sheet melt is occurring per year, and sea level has risen a total of 104mm since 1993 alone. Data of global temperature anomaly is tracked by NASA is shown in figure 3.

In response to the growing dangers resulting of climate change, PV energy has emerged as a significantly more responsible method for generating electricity. As extreme weather events increase in intensity and frequency, alternative energy solutions are growing more rapidly than ever. While this is somewhat good news, the processes for fabricating PV modules remain somewhat energy intensive and the treatment for modules at end-of-life is often used as an argument against the technology. Perhaps even more important is to continue to find ways to reduce the cost of PV modules while improving

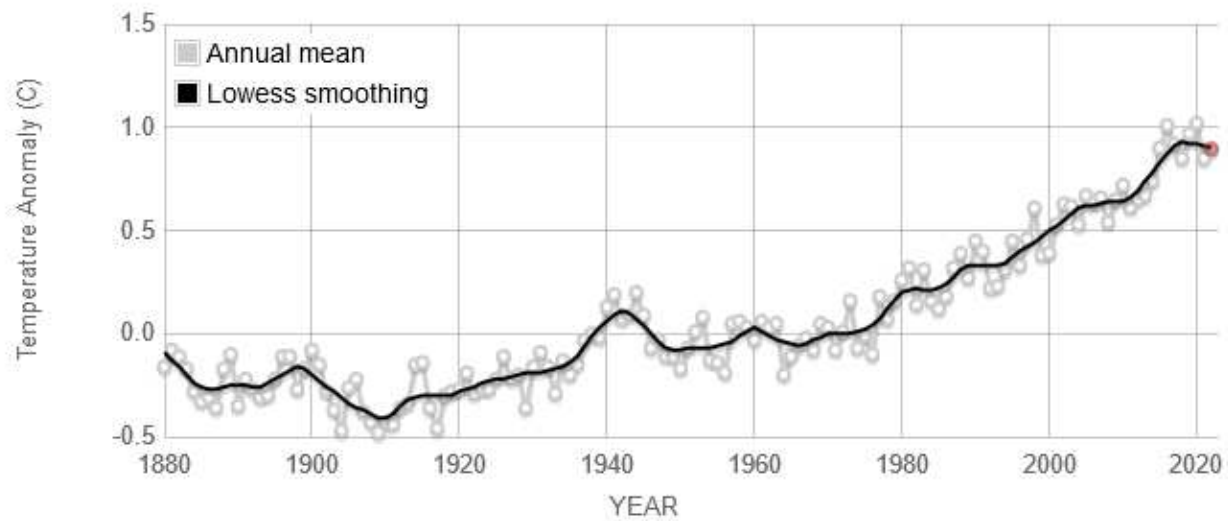


Figure 3: Data available at climate.nasa.gov of the global temperature anomaly since prior to the industrial revolution.

module reliability and longevity. The PV market is one of the fastest growing markets on the globe with around 13% year-on-year growth (Ahsan, 2019). As costs continue to drop in terms of electricity generated by PV, the technology has surpassed all other forms of energy generation in terms of cost per watt generated by the power plant (Amine, 2022). Because technology is not only necessary for the security of the planet, but also now one of the lowest-cost methods of generating electricity, growth of

the PV industry has become one of the most important topics to understand. The technology outlined in this research sets the ambitious goal of providing the big three. Improved cost, improved reliability, and good performance. While improved cost is outside the scope of this research, it can be surmised that the elimination of costly vacuum lamination is a significant enough factor to make that claim. This claim also has a significant amount of prior research which will be discussed further in chapter 2. Key issues for reliability, end-of-life treatment, and performance are discussed and tested. Meeting these goals has the potential to further the competitiveness of PV electricity generation which is already on a steep growth rate of wind and solar shown in figure 4 below.

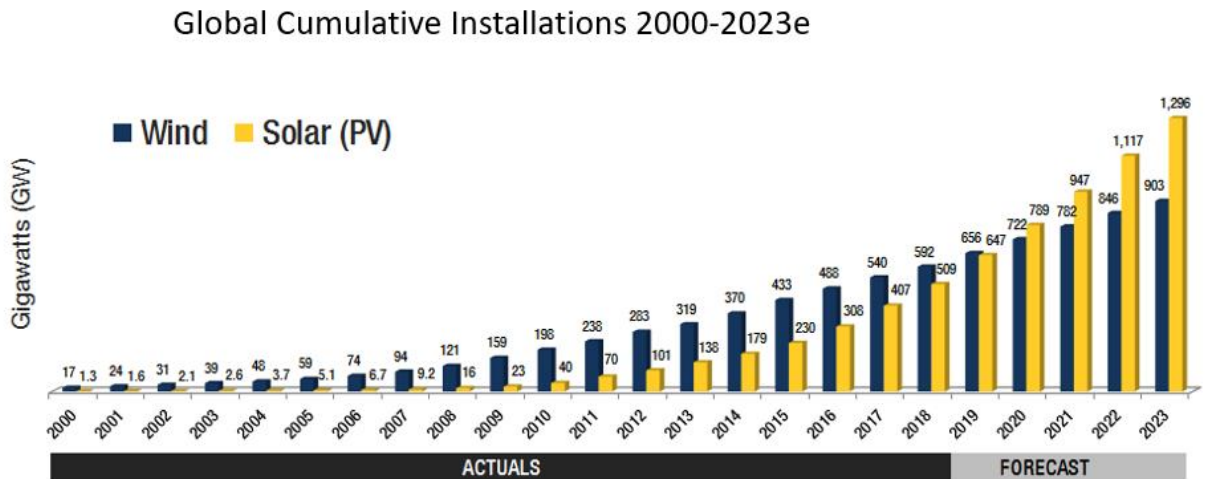


Figure 4: Yearly increase in cumulative global installations of PV and Wind since 2000 provided by NREL.

1.3 Hypotheses Identified and Research

In order to determine whether the proposed module architecture has potential for success, it is important to identify key questions to ask which can be researched and tested. It is also important to define clear metrics for if these hypotheses tested have passed scrutiny and what research remains to be accomplished. A brief discussion on the metrics of each test to be conducted and how this is measured is outlined here. Manufacturing equipment and samples fabricated are further discussed in their respective sections in Chapter 3.

1.3.1 Hypothesis 1:

The first hypothesis discussed earlier relates to bringing the leads through the sides of the module rather than the rear. Traditional modules utilize a junction box at the rear of the module which is a known potential moisture ingress path (Wisniewski, 2018). This rear junction box requires a hole to be cut in the rear glass of glass-glass modules and can be a weaker mechanical point. By applying PIB around the leads at the edge of the module, MEL has iterated this concept over a large quantity of samples and developed a series of best practices and processes which enable the ESM to be assembled more quickly and without a hole in the rear of the glass. For example, the leads are easily moved within

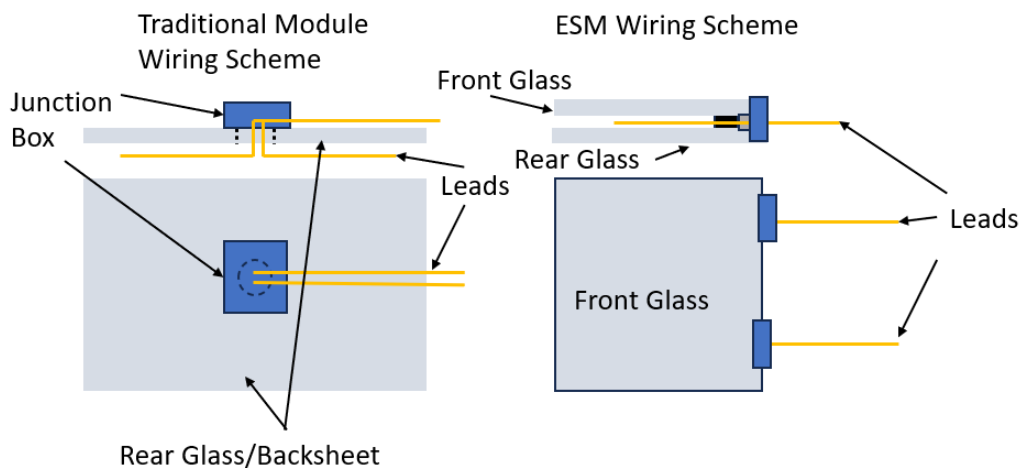


Figure 5: Traditional module wiring scheme (left) versus ESM wiring scheme (left). The wires in the ESM wiring scheme are brought through the edge of the module between the layer of PIB and silicone is injected around the edge of the wires.

the PIB which through destructive inspection of test samples has been revealed to lead to voids within the edge seal itself. This was solved by placing a clamp around where the wire exits. This clamp can be utilized in conjunction with a side-junction box. It may also shorten the length of wires necessary in PV energy generation compared to traditional module manufacturing. Differences between typical rear junction boxes and the ESM proposed method for bringing the wires out are pictured below in figure 5.

This is primarily tested under damp heat (DH) conditions since it replaces one moisture ingress point (the rear junction box) with another, which is the leads being removed from the sides. This experiment is conducted in a humidity chamber at a temperature of 85C and a relative humidity of 85% relative humidity. Three different optimized samples are tested by NREL and are inspected approximately every 1,000 hours of exposure to the DH conditions. These samples each contain a moisture indicating desiccant strip which will turn pink at varying degrees of humidity levels. Since diffusion is assumed to be high, this indicates if humidity has broken through the edge seal and can impact a c-Si. The first humidity level which can be indicated has indicators from 10% to 60% at 10% intervals. The standards outlined in IEC 61215 require modules to pass 1,000 hours in these conditions. While this is a considerable length of time, it is important to note that there are some significant benefits to increased longevity of PV modules as this will greatly reduce the net cost of electricity over the lifespan of the module. 50-year equivalent is chosen since it represents a doubling of the 25-year lifetime which traditional modules are expected to last. The acceleration factor for a humid climate such as that in Miami or Bangkok was determined that 5,000 hours was approximately equivalent to 50 years in such an environment (Kempe, 2022). This is also particularly significant since it is currently the Department of Energy's goal to double the current lifespan of the module (Barth, 2018). Rather than shaping a goal which meets current industry standards, future DOE goals are identified in harsh climates.

1.3.2 Hypothesis 2:

The second hypothesis concerns the ability for the module to be disassembled easily enabling the recovery of high value recyclable materials. This hypothesis brings up new challenges since it is quite clear that the current recycling method involving chemical separation is in fact significantly more complex (Dent, 2019). In fact, papers such as those outlined in Chapter 2 tend to gloss over the topic as an automatic given rather than delving into precise methodology for determining success in this area (Wirth, 2015). This thesis instead looks at the manufacturing process for defining the goals. In previous

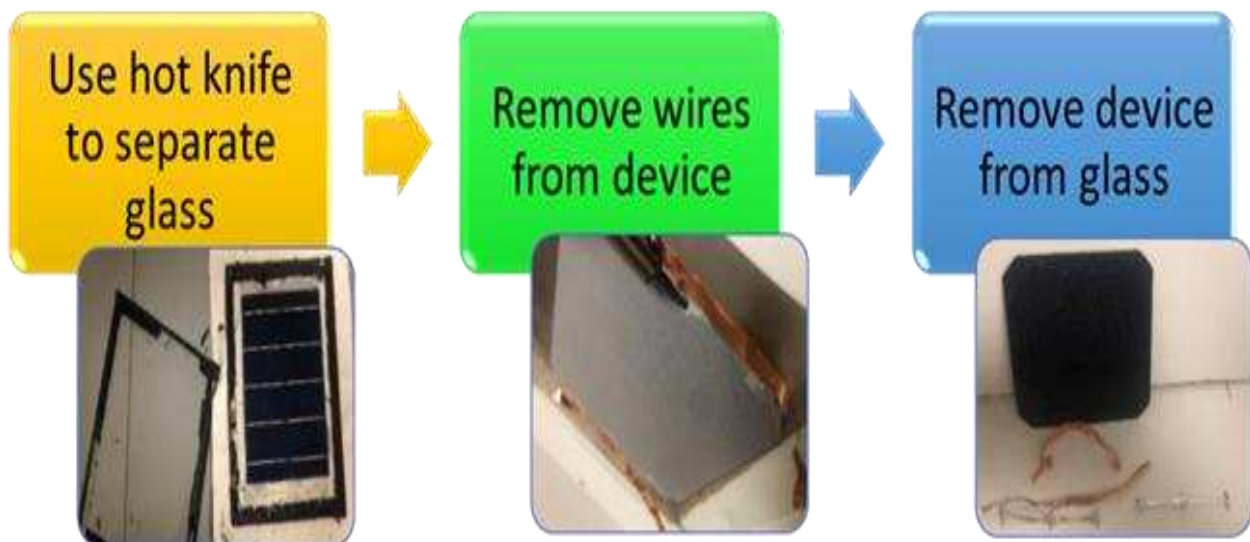


Figure 6: High-value recycling process steps for module disassembly with components completely separated.

work done by MEL, each step of encapsulation was demonstrated to take less than 30 seconds (Barth, 2018). Three steps of the process are defined to complete the encapsulation of the solar modules. The first is the application of PIB, the second is the application of silicone for the edge seal, and finally the module is pressed together. This means a module of 60cm x 120cm could potentially be produced every 30 seconds. Rather than attempting to define an arbitrary benchmark, the benchmark for disassembly can be to match the assembly process itself.

1.3.3 Hypothesis 3:

The third hypothesis identified is that the module can minimize beyond the detection limit the formation and growth of microcracks. This is a key issue which has been identified in traditionally encapsulated modules where harsh process conditions followed by the thermal cycling of a sandwich of materials causes microcracks to form and grow over the lifespan of traditional modules. This has been identified as a significant issue in terms of reliability and longevity of c-Si module architecture. In the case of MEL's novel encapsulation methods discussed here, process temperatures as well as pressure is significantly reduced. On top of that, the air gap in the module allows the c-Si cell itself to expand and contract unrestricted by the surrounding materials such that it is not cycled through stresses to the extent that cells which are traditionally encapsulated. This is suspected to prevent not only the initial

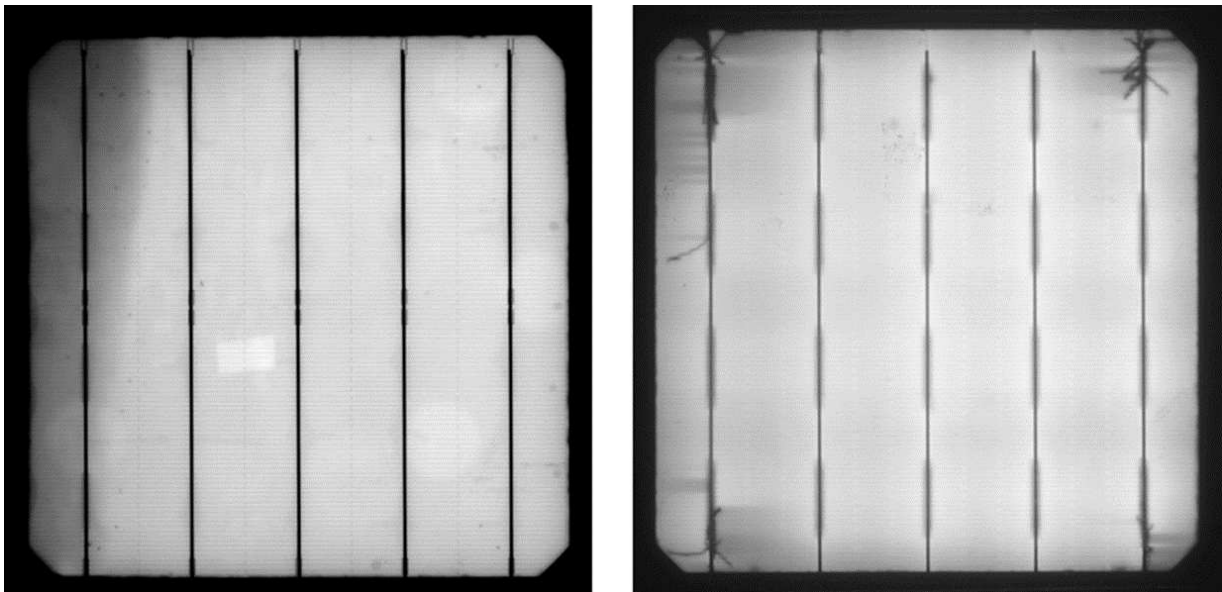


Figure 7: Electroluminescence (EL) image of ESM Module (left) no microcracks formed during encapsulation. Traditional glass-glass module (right) with formation of microcracks.

formation of microcracks, but also further growth of microcracks during the lifespan of the module.

Sample modules have undergone accelerated stress testing which simulates an accelerated lifespan of PV modules, and their performance is measured through a series of tests which are outlined in Chapter

3.

1.3.4 Hypothesis 4:

The fourth and final hypothesis identified is MEL's module architecture for c-Si can match the power of traditionally encapsulated c-Si modules. This has been discussed somewhat at length in section 1.1 since it is one of the more significant issues. There is also consideration for the optical analysis which will be discussed in section 2.3. Samples are fabricated which mimic both traditional module architecture and the novel module architecture developed at MEL. These samples are then numerically corrected for test conditions versus real-world incident light conditions at a 45-degree incident angle to the earth which are referred to as Air Mass 1.5 (AM 1.5). This is because AM 1.5 is the standard testing for watt peak in terms of comparing solar energy performance (though there is some nuance based on testing conditions which will be discussed throughout this thesis). The data generated is then directly compared to determine if there is any statistically significant difference between the current.

Chapter 2: LITERATURE REVIEW

2.1 Introduction

In this section, the motivation for the importance of this research will be explored. The intent is to form a narrative of what research has been done up to this point and to explore what is important to learn in the future. Encapsulation techniques, which do not utilize vacuum lamination techniques, are not in and of themselves novel to the PV industry. In 2007, Abound Solar was formed as a spinoff from MEL which was intended as a large-scale manufacturing and commercial sales company. Abound Solar utilized a module package design which did not use lamination or EVA encapsulation materials (Barth, 2009). This is the first attempt to commercialize ESM architecture, and it was shown to have a significant number of benefits compared to traditional module encapsulation. This novel technique had significant cost benefits when compared to other module architectures since it avoided the vacuum lamination process. This is outlined in “Abound Solar’s CdTe module manufacturing and product introduction”, a paper published for the 2009 Institute of Electrical and Electronics Engineers (IEEE) Photovoltaic Specialist Conference (PVSC). This thesis goes into detail about the manufacturing process and potential benefits of non-vacuum encapsulation techniques (Barth, 2009).

A few key primary benefits are highlighted in terms of manufacturing cost such as direct material costs, overhead, and manufacturing equipment and it was estimated that Abound Solar could have produced modules at around \$1.00 per watt. Other key highlights were the reduction in energy required for production, water, and greenhouse gas emissions (Barth, 2007). These results of Life Cycle Analysis (LCA) are independently verified by researchers at Michigan State University (Pacca, 2005). This work is continued in several papers written at MEL and NREL. This module had also passed International Electrotechnical Commission (IEC) 61215, a list of international standardized tests which a PV module must pass in order to be certified for use or sale.

2.2 Previous Adaptations for c-Si

While the original non-vacuum encapsulation technique was developed for Cadmium Telluride (CdTe) circuit plates, silicon has an additional challenge which adds a layer of complexity. This can be understood based on how layers vary between architecture required for c-Si versus CdTe. Since CdTe can be directly deposited onto the glass, there is no concern over optical properties, whereas c-Si is produced in individual cells which are not directly in contact with the glass. One of the primary benefits

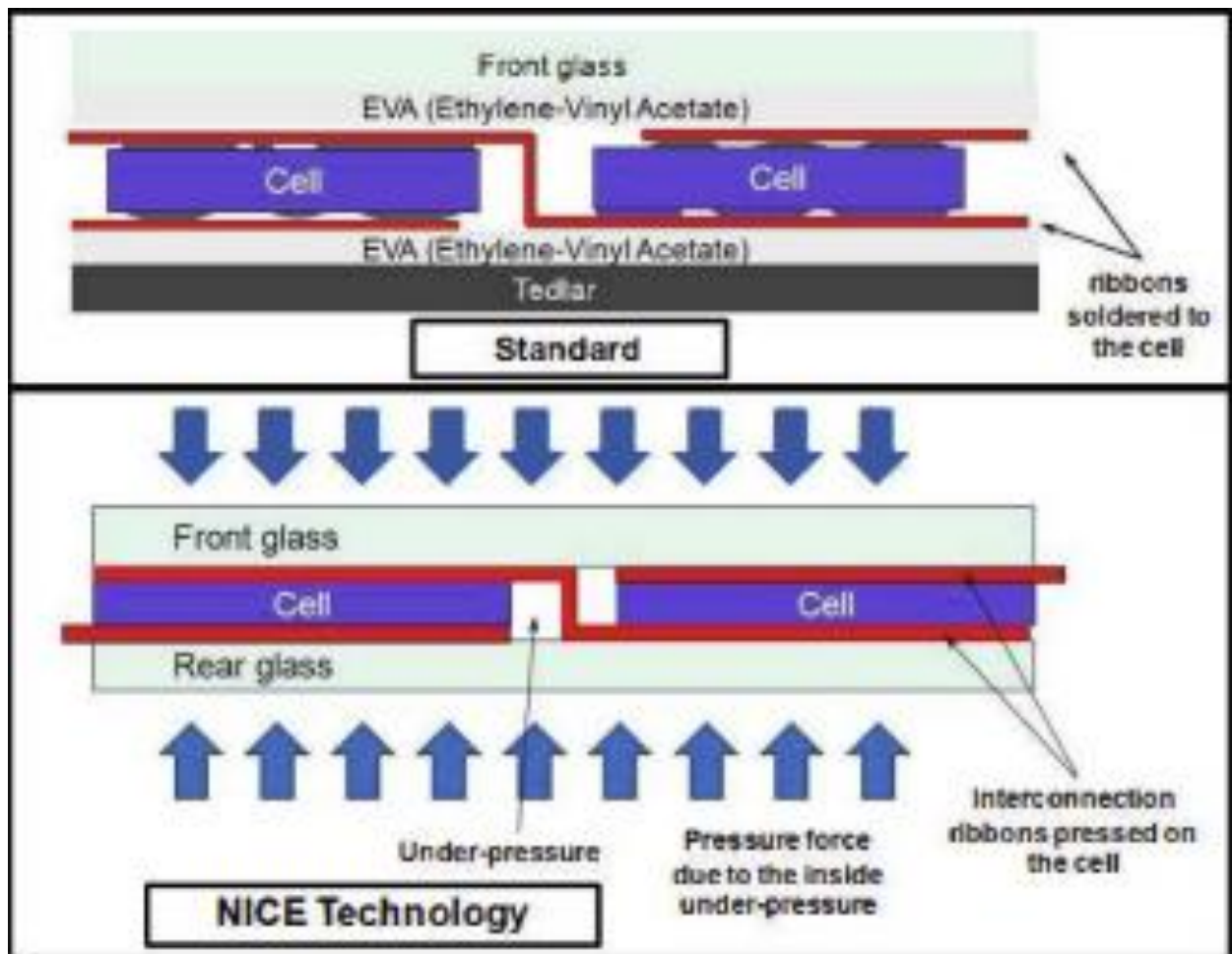


Figure 8: Schematic comparison of the standard module architecture (top) and NICE module technology (bottom) (Dupuis, 2009).

of traditional module encapsulation is that by utilizing lamination which has a similar index of refraction to that of the front glass of the module. Without the use of vacuum lamination, c-Si modules have an inherent challenge to match the power of traditional modules. These ideas are explored in papers which

originate from Fraunhofer in Germany and by Appolon Solar in France. The primary difference between the different module architectures is shown in figure 8.

The technology adapted for c-Si modules by Appolon Solar is named NICE (New Industrial Solar Cell Encapsulation) module technology and is overviewed in the paper “NICE module technology – From the concept to mass production: A 10 years review”. In this paper, the history of the NICE modules is explored and are similarly based on insulating glass (IG) technology shown in figure 8. This technology does not utilize EVA but instead contains an air gap between the cell and the front and rear glass. The cells are held under pressure in order to hold the tabbing ribbons in place rather than soldering them together (Dupuis, 2009). The paper presents the benefits of this type of encapsulation such as lower cost and increased robustness against degradation mechanisms such as moisture ingress and reduced microcrack formation and growth. The paper also notes the findings from the utilization of anti-reflective (AR) coatings on the cell and glass could be utilized to make up for the loss in power due to the poor optical coupling between the various layers. This issue is described in the paper as an optical discontinuity in the module which decreases the power by 7-10% (Dupuis, 2009). An ideal AR coating is modeled on the front and rear of the front glass as well as on the top of the c-Si cell which the paper reports as gains of 1.9% from the cell and 8.2% gains from both sides of the front glass having AR coatings [Dupuis]. This review provides a good overview of the important topics which should be covered when developing a deep understanding of IG based PV modules for c-Si, but it is also important to take a deeper look at some of the specifics. While many of the conclusions can be confirmed, one of the most important topics is optical losses. For instance, while the 7-10% losses are quite reasonable (confirmed by LED testing in section 4.5), one of the primary issues is that while 8.2% can be gained from a double-sided ideal AR coated glass, only 4.1% of that could be claimed as being able to benefit this technology specifically since any PV device could utilize an AR coating on the front of the front glass.

Neglecting half the claimed gains from the AR coating on the glass itself then implies a power reduction of 1-4% relative which could be a significant loss.

2.3 Optical Analysis

Digging deeper into work completed for the vacuum lamination free style module architecture a paper entitled “Encapsulant for glass-glass PV modules for minimum optical losses: gas or EVA?” is referred to by the overview details key results show that this power differential is also interestingly dependent on the spectrum emitted by the testing equipment. Since AR coatings typically perform better under visible light and tend to reduce performance under IR conditions, it is reasonable to assume that performance of the modules would be dependent on incident wavelength. If the test conditions are significantly different from real world conditions, this is likely to give an error in the performance of some modules versus other modules (Couderc, 2017). This has some more significant implications for materials which are dependent on the bandgap as the wavelength is a more significant factor in determining the net power output for each individual module. Since c-Si has a band gap of around 1.1

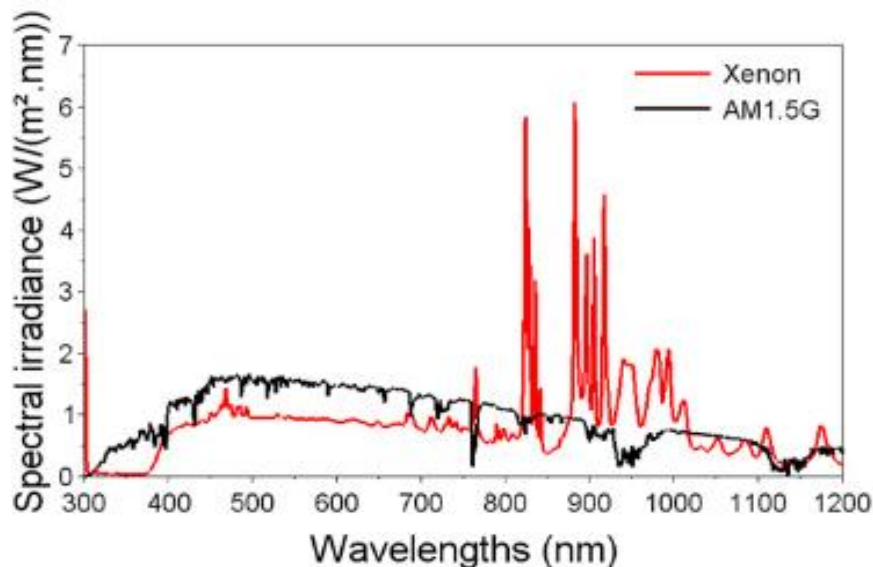


Figure 9: Spectral emission of typical unfiltered Xenon lamp compared directly to AM1.5G as a function of wavelength [Couderc, 2017].

electron volts (eV), the light which can be converted to electricity reaches the 1100 nm range (though somewhat beyond, however there is a significant drop off in this region). This paper is written in collaboration between the University Claude Bernard Lyon and Appolon Solar and focuses on exploring key differences between the performance measurement under Xenon lamp conditions and AM1.5G. The paper numerically calculates each layer of the structure for reflectance as a function of wavelength with AR coatings thickness and index of refraction optimized for peak visible light [Couderc, 2017]. The transmission of photons is then calculated as a function of wavelength and total light transmission is found through this process numerically. The paper finds that losses under AM1.5G are possibly even improved with internal AR coatings on the rear of the front glass and the front of the c-Si cell through a vacuum lamination free style of architecture compared to traditionally EVA encapsulated modules. However, it is important to note that these AR coatings are somewhat fine-tuned in a computer simulation for the purposes of this numerical modeling. In other words, these idealized AR coatings are not necessarily available, but are ideal hypothetical AR coatings which could potentially optimize the performance of this type of module.

Turning to Fraunhofer institute, the paper “TPEDGE: QUALIFICATION OF A GAS-FILLED, ENCAPSULATION-FREE GLASS-GLASS PHOTOVOLTAIC MODULE” is also valuable reading for understanding the benefits and drawbacks of this type of encapsulation strategy. Unlike Appolon, cells are held in place by polymer pins which adhere to the cell directly to the back glass. Additional polymer pins are placed on top of the cell in order to prevent cells from contacting the glass itself [Wirth, 2015]. This contrasts with Apollon’s NICE module technology of utilizing pressure from the glass. This architecture is referred to in the literature as TPEdge. The TPEdge module is shown to be more resilient to potential induced degradation (PID). It also passes a thermal cycling (TC) test of 400 cycles (-40C / 85C), 2000 hours of damp heat (DH) at 85% relative humidity (RH) and 85C, Hot Spot endurance Test in accordance with IEC 61215, and a mechanical load test under a load of 2400 Pa mounted with back rails

[Wirth, 2015]. The paper does not mention the humidity freeze test from IEC 61215, which may be an important factor (see section 4.3).

2.4 Mechanical Advantages

Previous work mentioned thus far represents a significant overview of the technology and the potential benefits as well as the challenges which face a non-vacuum lamination architecture for c-Si modules. Much of the reasoning for this type of architecture relates to lowering cost and improving reliability. Reducing the amount of material reduces the cost, but reliability and longevity may also be equally important factors. “Numerical simulation of the evolution of stress in solar cells during the entire manufacturing cycle of a conventional silicon wafer based photovoltaic laminate” takes a deeper look into the stresses which happen during the encapsulation process for traditionally laminated cells through numerical methods. Microcracks can be formed during the encapsulation process in traditionally manufactured cells due to the non-uniformity of pressures placed on the cell during encapsulation. The pressure varies numerically and is accounted for during preheating, evacuation of air, pressure-ramping, curing of the EVA, and post-lamination cooldown (Song, 2022). The paper finds that along the busbar ribbons, a maximum principal stress of 275 MPa are found along the rear of the cell, making for a significant likelihood of crack formation along a critical point where the cell is being stressed [Song, 2022]. This modeling is backed up by papers such as “Probing stress and fracture mechanism in encapsulated thin silicon solar cells by synchrotron X-ray microdiffraction” which utilizes synchrotron X-ray microdiffraction (SXRD) to probe microstresses in c-Si at various steps during the lamination process.

2.5 Moisture Ingress Modeling

There has been a significant amount of work done at NREL in terms of modeling moisture ingress for PV modules. Since the modules being designed are of double-glass type, the ESM is designed in accordance with these results. Early work on this shows that specific material around the edge performs

best under these conditions and can be improved with additional desiccant which absorbs moisture even further (Kempe, 2005). This early work uses a simple 1-D model to show moisture breakthrough through the edge seal of a few different materials such as Aclar in use for modules which are of glass-glass construction, however, these breakthrough times are determined to be without desiccant carried in the edge seal itself (Kempe, 2005). Data in this early work is taken for environments such as Miami in order to determine acceleration factors for DH, however, is refined significantly with a 2-D model for modules which do not utilize a laminate on the interior (Kempe, 2023). The most recent work available is possible due to improved material selection (Shimpi, 2019), which shows that PIB with desiccant is the best material for the outside edge.

Literature from 2023 is then the combined effort between NREL and the MEL in terms of designing a module which can improve modules with an edge seal for CdTe type devices since CdTe is more susceptible to degradation due to moisture. 10 separate modules designs are modeled utilizing finite element analysis for CdTe modules which are compared to each other in terms of moisture ingress modeling for varying regions such as Bangkok and Miami. Again, this is based on meteorological data which is collected by hour over several decades. This allows for a time step of one single day over a period of 25-50 years in each environmental condition utilizing a characteristic humidity and temperature for each day. These models are then compared to DH conditions of up to 5,000 hours and compared to each other (Kempe, 2023). It is important to remember that these designs are somewhat module design dependent. 5,000 hours of damp heat does not necessarily equate to the same acceleration factor for a typical c-Si module with a polymer backsheets which does not utilize glass at the rear and is similarly not equivalent to a module which does not utilize a perimeter seal of some sort overall. This is because of how the varying moisture pathways work depending on the materials of which moisture can enter. It is therefore key to identify which module architecture modeled matches the design, or rather, to design the module such that moisture ingress is best reduced under humid

conditions. The ESM module design is most representative of one particular module design for CdTe which shows the best use of perimeter seal and internal desiccant load. The rate for which moisture breakthrough occurs is based on an infinite series which converges of several terms and is referred to as the Water Vapor Transmission Rate (*WVTR*). This value is calculated numerically and tabulated in the collaborative work between NREL and CSU (Kempe, 2023). This is then compared to environmental data from Bangkok and Miami using the same model parameters, for these regions with modules utilizing and edge seal, 5,000 hours equates to approximately a 50-year lifespan in terms of moisture ingress (Kempe, 2023).

2.6 Recent Publications

Research has been ongoing at MEL to best develop this type of module architecture. This includes the continued work of Kurt Barth and the encapsulation laboratory at MEL. Publications relating to the strength benefits of the module architecture. Analysis has been conducted at MEL in order to demonstrate key strength components of the novel module architecture. Many samples are fabricated without circuit plates and undergo a number of tests (Shimpi, 2019). Much of this work describes the process optimization and is utilized in finding optimal process conditions. The materials selected are also based off previous work done by the laboratory at MEL (Ellis, 2020). This work outlines the robustness of the module architecture to strength testing, thermal cycling, creep testing, as well as resilience against hail damage. In this work, it is shown that the module architecture with no circuit plate is well-suited for testing mechanical properties since the circuit plate is not directly connected to the glass mechanically.

In collaboration with NREL and MEL, models have been created to show the robustness of this module architecture as intended with a typical rear junction box, can withstand a significant amount of damp heat exposure. In work by Mike Kempe, he determines an acceleration factor of 5,000 hours in damp heat (conditions at 85% humidity and 85 degrees Celsius) to be equivalent to 50 years in harsh

climates such as Bangkok. Further work in collaboration with NREL has shown that this module

Advantages of Perimeter Seal Module Architecture for c-Si

Mechanism/ Engineering Challenge	Lamination Modules	CSU Architecture
PID	Yes	No
Yellowing (Acetic Acid Buildup)	Yes	No
Delamination	Yes	No
Backsheet Failure	Yes	No
Cell/interconnection Corrosion	Yes	Less Probable
Moisture Ingress	Less Effective Moisture Barrier	Reduced For Longer Lifetime
Stress During Encapsulation	Heat Expansion Stresses Devices	Reduced Microcrack Formation for Longer Lifetime
Recyclability	Difficult to Separate Device from Glass	Separation of Materials Significantly Simplified

Figure 10: Comparison of various degradation mechanisms experienced by solar modules between traditional lamination modules and CSU’s ESM module architecture.

architecture has many potential benefits as discussed in various meetings. A chart was prepared by collaborators with NREL which goes into further detail of the known and potential benefits of ESM technology developed at CSU and is shown in figure 10.

Most recently, this collaboration has led to some significant progress in this type of architecture. Key findings are discovered in a paper which is currently a manuscript in preparation for publication through the IEEE PVSC (Ruhle, 2023). This paper details much of the work done to demonstrate the reliability of the module and reduction of specific degradation modes. For example, samples in this work are tested for 2,000 hours under a high voltage which tests against potential induced degradation (PID). It is understood that one of the primary mechanisms of PID is that sodium ions can be transported across the glass and through the EVA. ESM samples performed significantly better under PID testing than traditional modules. This work also highlights some of the potential longevity benefits and goes into detail on the progress for c-Si ESM modules and their ability to match power to traditional vacuum

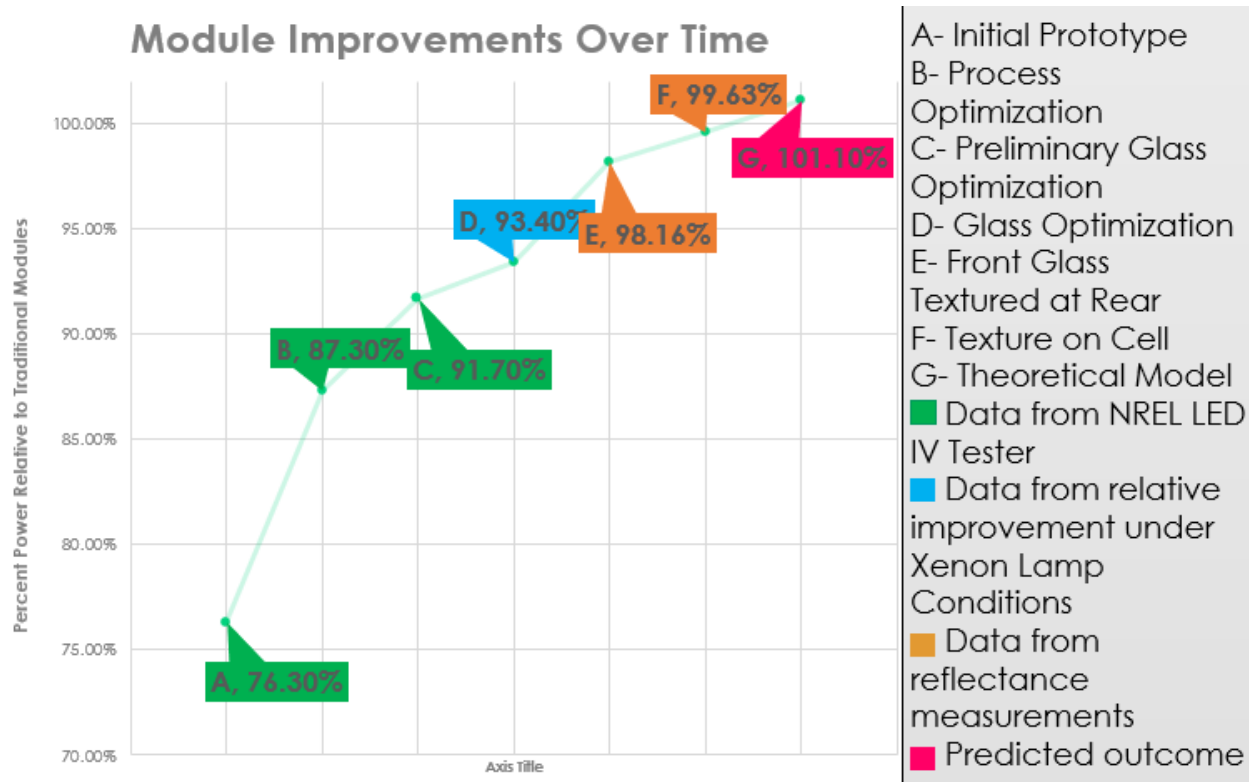


Figure 11: Depiction of progress improvements in matching power to traditional modules. 100% is a 1-1 match for idealized power.

lamination modules. A progress map for matching power is given in the future work section outlined in figure 11. Cell selection is also discussed, as there is a lengthy discussion on the circuit plate makeup and how that impacts UV exposure. While this module experiences UV degradation within limits of current industrial standards degradation, some cell architectures are found to be more resilient against UV. This is a valuable finding since many typical EVA's utilize UV blockers which prevent UV degradation. Modern modules are moving away from blocking UV light since this extra light can be converted into power if degradation is minimized through cell construction. One of the primary factors is that many of the cells utilized in testing were of an older vintage which utilizes boron dopants which are susceptible to UV degradation. Modern cells are moving towards gallium dopants which are not as susceptible to UV degradation. In discussion with NREL, there are some cells which are almost entirely resilient against UV degradation and have been identified as potentially better cells for future testing. Combining the

findings of previous work and moving forward, this thesis will continue the work being accomplished at MEL and follow along with next steps outlined in the most recent publications (Ruhle, 2023).

Chapter 3: EXPERIMENTAL DESIGN

3.1 Introduction

Due to minor design changes based on best practices and improvements to the simplification of the overall module design, it is valuable to test samples of this module under key test conditions. This section will focus on demonstrating some of the claims being made about this architecture which may need continued development and testing. Tests are designed to address the challenges with developing new technology in accordance with benchmarks set for whether a hypothesis is accurate or not. This section will discuss the equipment, samples, and experiments conducted as well as go over the metrics utilized for the hypothesis outlined in the section which were defined in section 1.3. Each of the four hypotheses are outlined as separate experiments rather than a singular experiment. While some of these experiments are more straightforward, others, such as the experiment to determine if Isc can be matched is slightly more complicated. Each experiment will then be followed up on in Chapter 4 which will discuss the results of the experiments conducted thus far.

3.2 Equipment and Sample Manufacturing

The Encapsulation Lab at MEL is a state-of-the-art facility which is capable of prototyping PV module architecture at a rapid development rate. The main facility equipment can produce module architectures up to 60cm x 120cm in size and has been adapted to produce a variety of smaller size modules depending on the testing apparatus for which the samples can be measured in. In collaboration with NREL, MEL's facility has developed a series of prototype samples which can be utilized for accelerated stress testing in accordance with industrial standards outlined in IEC 61215. Individual tests which are specific to hypotheses mentioned in Chapter 1 are specified for each specific hypothesis later in this chapter.

3.2.1 MEL's Manufacturing Equipment:

The main manufacturing equipment at MEL features a state-of-the-art edge seal tool with dual dispensing nozzles. This machine takes the place of complex vacuum lamination used in traditional module manufacturing and is capable of emplacing both the PIB component and silicone component of the edge sealed module in under 30 seconds per process step for a 60cm x 120cm module shown in 14. The tool hardware configuration is shown in figure 13. This equipment was specially designed for IG technology and was adapted for use in PV manufacturing through DOE funded projects. It is ran by MEL's



Figure 12: Graco supplied heated PIB pumping system (left) and polymer application tooling shown with 30cm x 30cm adapter plate installed (right).

encapsulation lab team and has been modified in order to produce many different sample sizes depending on the needs of the prototype and constraints for testing. The process for the edge seal application were optimized utilizing statistical design of experiments (Ellis 2020, Shimpi 2022). These results are utilized to better rapidly optimize for varying sizes of prototype modules for rapid turnaround.

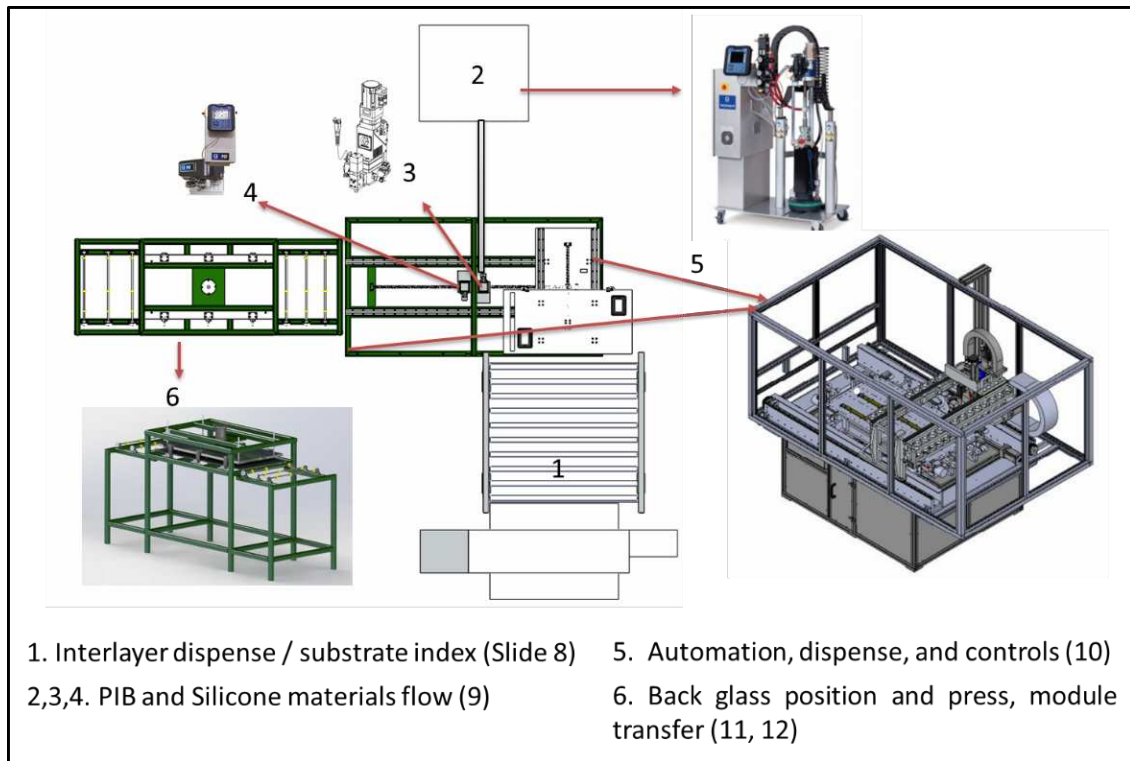


Figure 14: Tool hardware configuration.



Figure 13: Image of pneumatic press utilized at MEL.

The facility also utilizes a press which has an adjustable pressure. It was also modified to have

additional pistons which improve the uniformity of press for 60cm x 120cm modules while also providing uniformity directly under the press for modules which are square such as 20cm x 20cm and 30cm x 30cm. Press conditions have been optimized in previous work and are developed at MEL. For this, press condition optimization is done through a statistical design of experiments (SDOE). This allows for the application of PIB as well as the press conditions for PIB to be properly tuned together. Over 50 samples have been fabricated with either glass only or glass and circuit plate during this process optimization. By taking careful notes and records during each sample production run, data can be utilized to reduce the process optimization time for material changeover as well as variance in sample size and dimensions.

3.3.2 Sample Fabrication

The general procedure for sample fabrication developed at MEL is described in this section. Changes to sample fabrication for specific experiments are noted in their respective sections. A general

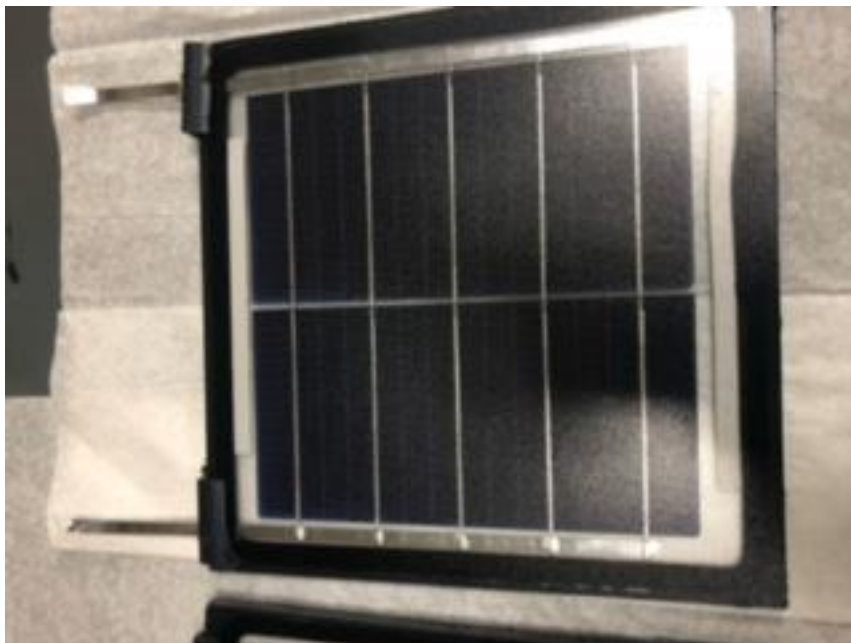


Figure 15: Sample fabricated by MEL for the purpose of accelerated longevity testing at NREL.

sample shown in figure 15. Multiple samples are fabricated over time with constant optimization for each consequent sample set fabricated. Sometimes, multiple improvements are made over a single set of module fabrication.

General samples do not use nanostructure on the interior of the sample unless otherwise specified. This will be covered more in depth in sections which deal with hypothesis 4 since these samples were made to match the power of traditional modules specifically. Process steps are listed below.

- Glass is cleaned prior to encapsulation.
- Back glass is placed on encapsulation tool.
- The first layer of PIB is placed on back glass.
- Back glass is moved to worktable.
- Dots of UV curing adhesive are placed on cell tabbing ribbons.
- UV curing adhesive is bonded to glass and wires to hold cells in place on the back glass with a UV lamp.
- The second layer of PIB is added to the sample which forms a layer which seals the leads which exit the module.
- Front glass is aligned onto the sample.
- Sample is pressed together based on previously optimized press conditions based on sample size and type of glass.
- Silicone is injected into the edge via a battery powered caulking gun which has a modified nozzle for better process control utilizing a process developed by MEL.
- Sample is cleaned of any excess material and examined for flaws.
- Samples which have little, or no observed flaws are sent to testing. If flaws are detected, they are carefully analyzed, and process conditions are noted and improved.

3.3.3 Testing and Measurement Equipment Used:

Samples are tested primarily at NREL. Some of the equipment is considered sensitive information and no images can be taken, in these cases the testing equipment and conditions will be described in as much detail as is possible. Testing is also completed in collaboration with NREL in order to maintain independent testing conditions as best as possible. This is accomplished through the NSF internship program which supplements research into renewable energy. Eight total tests have been accomplished through this collaboration with NREL and are listed below and will be described individually in this section:

- Current and voltage (IV) measurement
- Electroluminescence (EL)
- Photoluminescence (PL)
- Damp Heat Testing (DH)
- Ultraviolet accelerated stress test (A3)
- Thermal cycling (TC50)
- Humidity Freeze (HF10)
- Quantum Efficiency (QE)

Modules are tested at Tests conditions for damp heat are conducted at NREL in a sealed chamber which maintains a constant temperature of 85C and 85% Relative humidity. This equipment is certified and maintained by technicians at NREL and was available through use due to the NSF internship program. This test varies in time depending on the goals of the test. A3 testing is also conducted at NREL, this test involves a high-intensity UV lamp and environmental chamber. This simulates constant heat and



Figure 16: A3 testing chamber configuration. Test conditions are described in table 1 exposure to UV radiation. The acceleration factor is estimated to be that 2,000 hours is approximately 10 years equivalent of UV exposure (Kempe, 2023). The testing apparatus appears in figure 16. Testing conditions are available in the table below, table 1. The samples also undergo 50 thermal cycles. These thermal cycles are conducted at temperatures cycling between 80C and -40C. Samples are currently in line for additional cycling tests.

Table 1: A3 environmental testing chamber conditions

Variable	Irradiance @340nm	Irradiance @ 300-400nm	Chamber Temperature	Relative Humidity
Test Condition (Measured)	0.8 W/m ²	85.79	65.0	20%

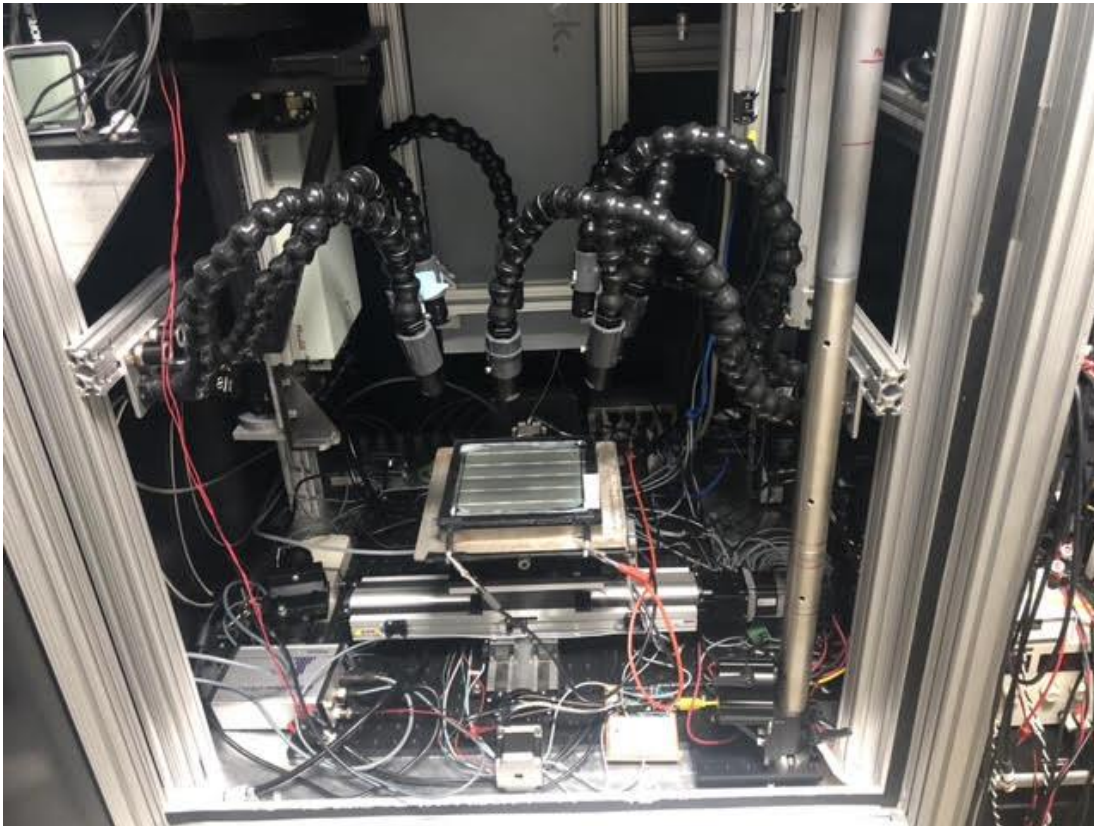


Figure 17: EL and PL measurement device in PL configuration. Each of the adjustable black arms are designed to emit a laser which is above the bandgap. This excites electrons and generates luminescence directly from the sample.

NREL was also helpful in the assistance of taking key measurements such as IV, PL, and EL imaging which is utilized in measuring the performance of samples before and after each accelerated test conducted. EL and PL imaging are utilized primarily to assess the formation and growth of defects on the cell. This made these imaging techniques particularly useful for determining the formation and growth of microcracks on samples fabricated. EL imaging is taken by running a current across the sample

circuit plate. This excites electrons above the bandgap which in turn emit photons of close to the bandgap energy and produces illumination in the IR region (about 1100 nm). Images of this phenomenon can be taken by a modern camera. In the case of PL imaging, electrons are excited instead by a laser which emits photons of energy levels above the bandgap. This similarly excites electrons to the across the bandgap into the conduction band which then emit photons of an energy level around the bandgap. EL imaging typically has a higher intensity of light and can be useful for more overall characterization of the sample, while PL imaging tends to be less intense which can be more useful for identification of smaller imperfections in the sample. The testing apparatus for these measuring techniques is shown in figure 17 in the PL configuration. Additional EL and PL images are shared in section 4.4 as part of the discussion of results.

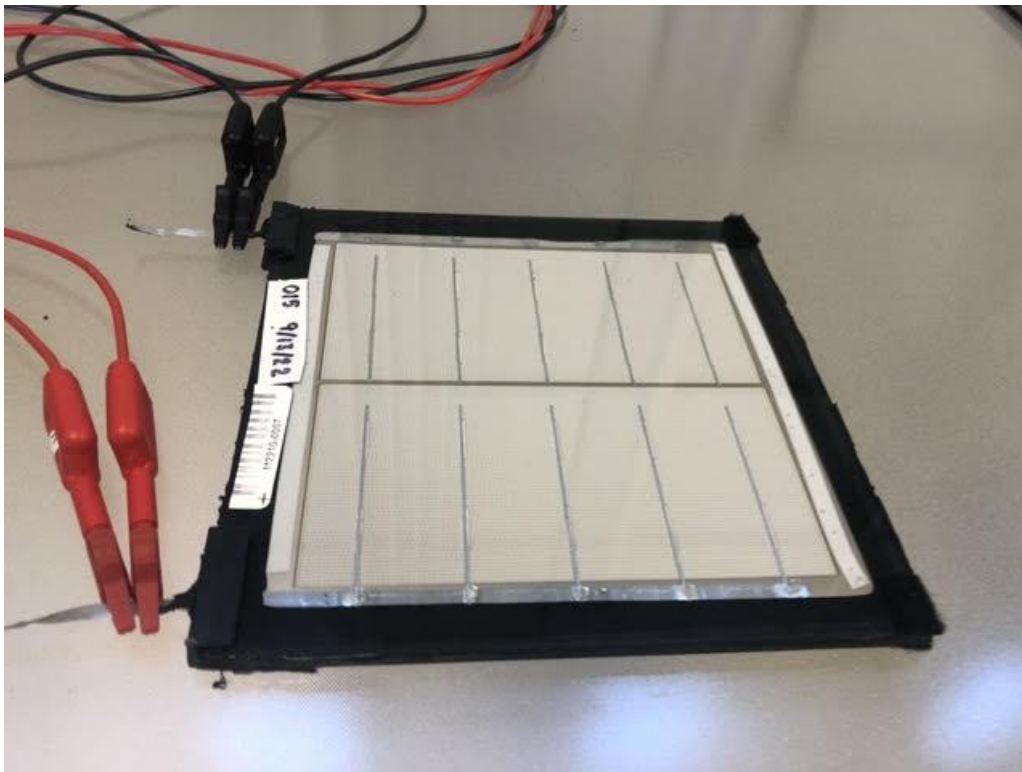


Figure 18: JV measurement device for xenon lamp at NREL in sample configuration.

IV measurements are made possible using both a Xenon lamp and when available a LED lamp. These are often referred to as “solar simulators”. IV curves show the relationship between output voltage and current of a PV module. Maximum voltage (I_{sc}) can be obtained when there is no voltage applied to the module while maximum current is obtained when current no longer can flow due to the voltage applied to the module. At a basic level, as the voltage applied across the module increases, current flow is reduced. The maximum power point can be obtained by multiplying the current I and the

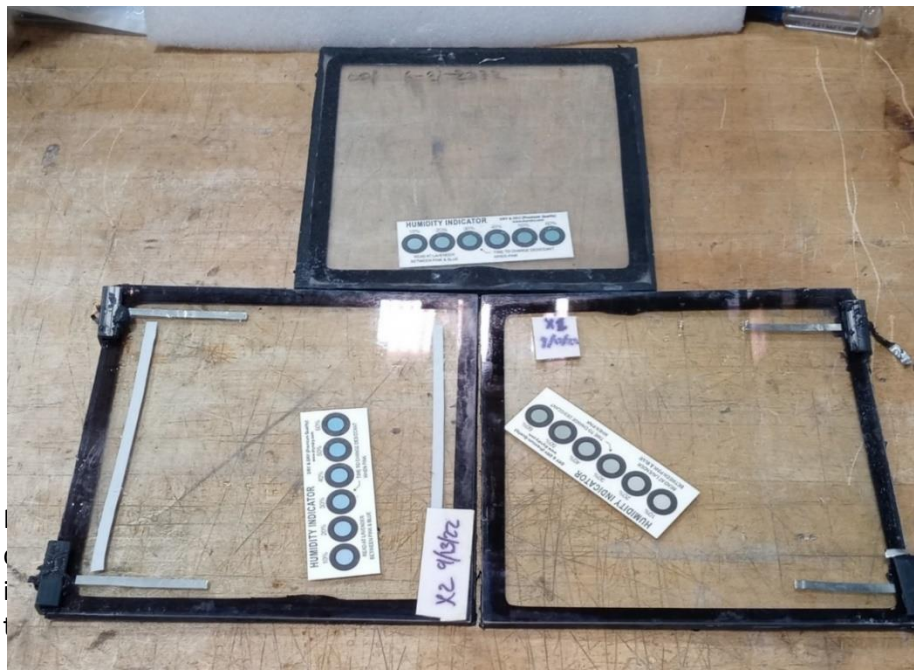
Figure 19: Xenon IV testing equipment available at NREL without Xenon solar simulator illuminated.

voltage V and finding the point at which these two variables multiplied together reach their maximum power point. The testing apparatus for IV characteristics is shown in figure 18.

QE data is also provided by NREL. This involves bombarding the sample with light across the solar spectrum and measuring the percentage of photons of each wavelength which are converted to electricity. A sample QE set utilized is discussed further in section 3.6. This is utilized to compare the response of traditional modules to light relative to the ESM samples which are fabricated at the MEL.

3.3 Hypothesis 1

The first hypothesis discussed earlier relates to bringing the leads through the sides of the module as discussed in section 1.3.1. Three different test samples are shown in figure 3 and prepared as



followed. Over 10 samples are fabricated for the purpose of optimization, however a limited number of samples actually go through DH testing due to equipment availability. This lack of number of samples tested is handled by ensuring that each sample is iteratively improved. It took several test samples to ensure that only best examples were sent through testing. An example learned over this iterative process was that the leads exiting samples needed to be clamped down. Moving leads within the PIB often led to voids in that area which provided a rapid moisture ingress pathway. By securing the leads with clamps on the edge it was made possible to prevent them from moving inside the PIB and forming voids. This and many other optimizations were completed before finalizing samples at MEL before sending for testing to NREL. One sample is made with no busbar ribbons extruding from the module architecture and no desiccant carrier, one sample is made with no desiccant carrier and busbar ribbons extruding from the module out the side, and one is made with desiccant carrier strips and busbar ribbons extending from the side. The key difference between these samples and sample fabrication described in 3.3.2 is that there is no circuit plate in use. The reason for this test is to demonstrate the necessity of the desiccant carriers inboard of the module to extend the life to 50 years in an extremely humid climate while simultaneously showing that the busbar ribbons exiting the side may be a moisture ingress point. While having the package designed in such a way in which the busbar ribbons may extend out the side may reduce overall cost, reduce complexity, and eliminate the failure point which is introduced by the traditional rear mounted junction box, it also introduces a new failure point at the location where a junction box would be mounted to this type of architecture. Research is conducted collaboratively between MEL and NREL with sample fabrication completed at MEL and sample testing completed at NREL.

3.4 Hypothesis 2

Research finds that the disassembly can be divided into three similar process steps as the assembly. This was initially discovered by utilizing a variety of readily available tools which are similarly

used in the IG industry. The first step in the process of disassembly is to separate the two pieces of glass, this was shown to be possible with a heated knife or by heating the sample first. Pre-heating the sample was able to yield significantly better results, however, this was likely due to consistency with hand tools which created challenges in yielding identical process conditions on varied attempts. For this part of the process, it was found that heating the module to 80C was the most effective method for separating the two pieces of glass. The second step was to remove the majority of PIB and silicone edge sealant utilizing an oscillating multi-tool with an attached saw-tooth on the edge. Varying sizes of saw-tooth pattern were utilized and the patterns which removed the most material easily were selected for final testing. By applying a light pressure with the oscillating multi-tool, the vast majority of PIB and silicone can be removed in a single pass with the tool. Since this tool could be easily automated, this was considered as a proof-of-concept for the disassembly of the module. Finally, the module must undergo a final cleaning step to remove any excess material which other steps did not completely accomplish. For this, the tool is changed to a hook-and-loop type tool with a scouring pad affixed to the end of the oscillating tool.

Each step is timed along a 200mm segment of glass from beginning to end with a stopwatch. Times are recorded onto a spreadsheet. As these processes were accomplished by hand, there is a significant amount of decay in the overall time each step took after each attempt. It is observed that this time reduction is not linear, but instead converges to a value as a decaying exponential would. This makes sense because these processes are being completed by hand rather than by a fully optimized machine, however, as technique improves, the value at which the data points are converging to is the optimized time which could be accomplished by a machine. This leads to an estimate of a total process time of 90 seconds for the total time it would take to disassemble a 60cm x 120cm module.

3.5 Hypothesis 3

The third hypothesis discussed in section 1.3.3 is that microcrack growth can be reduced to below detection limits due to lack of encapsulants which can apply stresses to the circuit plate. This experiment involved a multitude of accelerated stress tests which are considered useful in determining the real-world degradation of PV modules. These tests so far have consisted of 200 hours of exposure to damp heat (85C 85% RH), 2000 hours of exposure to UV radiation which will be referred to as A3 testing (peak irradiance at 340 nm – 0.8 W/m², Irradiance at 300-400 nm 85.8 W/m² 65C, 20% RH), and 50 thermal cycles. Tests are still ongoing, and modules will be placed in 10 humidity freeze cycles next. Module IV curves are taken to get a baseline of the sample performance. To measure the microcrack formation, Electro-Luminescence (EL) as well as Photoluminescence (PL). These images can be analyzed by finding the change in area of the cracks in photo imaging software. EL imaging functions by running a current through the PV device and taking an image of the device in the infrared (IR) spectrum. This is possible because the PV devices can operate as a light emitting diode (LED) when a current is run across them. PL imaging is somewhat similar, though rather than running a current across the device, a laser emitting higher energy photons than the bandgap is used to excite electrons and light can be collected around the bandgap which for c-Si is also in the IR spectrum at around 1100 nm. Areas where cracks have formed show up significantly darker than regions in which no cracks have formed because these areas are no longer functioning properly.

3.6 Hypothesis 4

The fourth and final hypothesis is that current can be matched utilizing interior textures. As pointed out in chapter 2, this has a few complications due to the nature of current testing procedures and availability of equipment. Previous research has found that LED lamps are a better representation of AM 1.5 than traditionally used Xenon lamps. However, it is difficult to attain access to a solar simulator

of sufficient accuracy. Since this test is somewhat rare, it is typically reserved to measure reference samples in order to properly calibrate the Xenon lamp testing apparatus. Since this technology relies on varying layers of texture which are optimized closer to the peak of visible light, this can create issues when it comes to comparing traditionally laminated samples against the novel module architecture. Samples are initially prepared with no interior texture and then tested at NREL utilizing LED lamps. After process optimization, under LED testing conditions, a drop of 8.5% in I_{sc} is observed compared to traditionally laminated samples. This is in line with findings from Fraunhofer mentioned in Chapter 2 of a loss of 7-10% without improvements made to the interior of this style of module architecture. Samples 003-010 are improved through process conditions and adjustments are made based on data to produce the best possible samples with this module architecture. More recent samples show greater consistency and measure like samples 009 and 010 when compared to traditionally laminated modules (next figure).

Once best practices are established, a process for optimizing the application of the interior nanostructure is also developed. Due to material constraints, smaller samples than the modules produced for the purpose of collaboration with NREL are created. These will be referred to as micro-modules. These are intended as simulations of the novel style of module encapsulation. This makes direct comparison on a small scale possible. With available Xenon JV equipment at MEL's PV

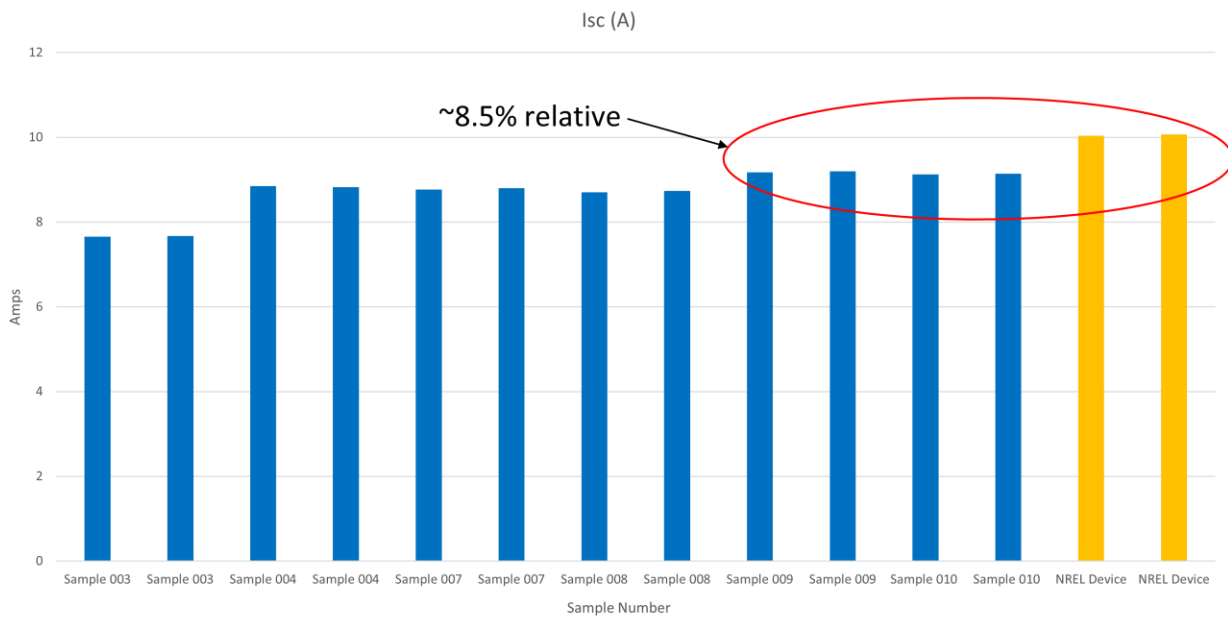


Figure 21: Sample optimization for process conditions taking place iteratively as best practices is established to create uniformity in production and best possible sample. An Approximate 8.5% relative reduction in performance in Isc is noted when testing under LED lamp conditions measured by NREL.

manufacturing laboratory, samples are compared to cells which are modeled off traditionally encapsulated cells. Since vacuum lamination equipment was not readily available for micro-modules, EVA is replaced with silicone oil which has a similar index of refractive index. One consideration to make

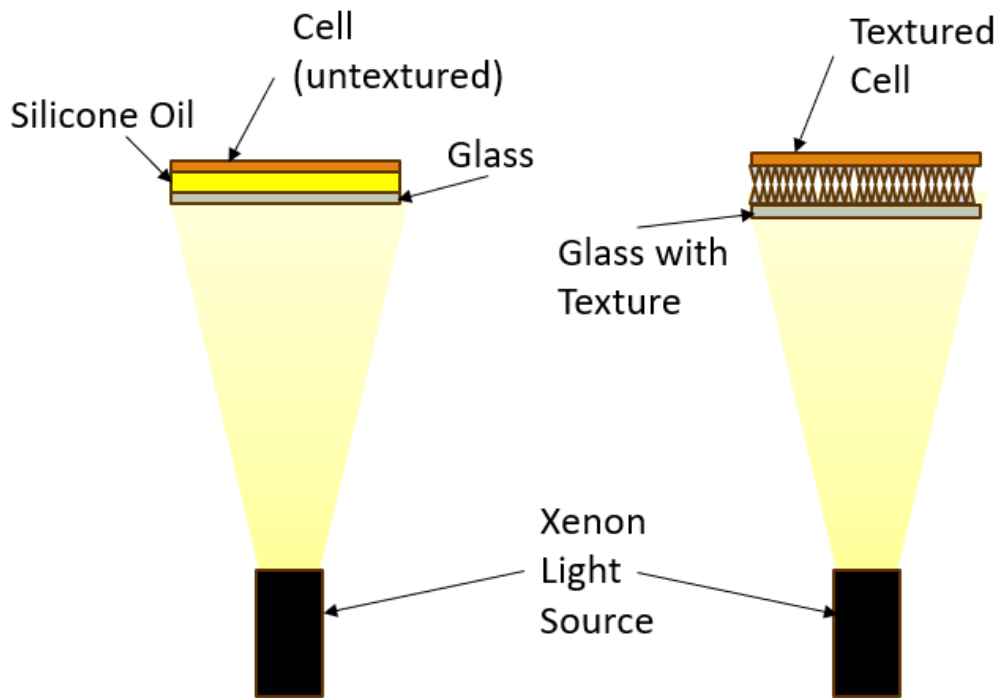


Figure 22: Experimental setup for testing tiny modules which are similar to traditional encapsulation (left) and MEL's module architecture. This design is not the full finalized design, but rather small cells which can fit in the available testing apparatus at the MEL.

is that silicone oil does not absorb UV to the same extent that typical PV EVA does. However, that is changing as c-Si cells become more resilient against UV degradation (Woodhouse, 2020). This can also be applied without voids within the makeshift encapsulant by hand when used in combination with a specialized glass provided by NREL. The micro-modules are assembled, optimized for best performance, and tested under xenon lamp conditions.

In order to adjust for the available xenon lamp conditions, reflection data is taken and carefully analyzed. This is done with the use of a transmission measurement device which has a spherical integrator. Each layer is carefully measured for reflectance per unit wavelength. Excess light that is emitted by the xenon lamp in each wavelength is then removed from the power output of the novel module architecture. This is numerically integrated across the AM 1.5 spectrum and corrected based on reflectance data taken at the MEL PV manufacturing laboratory. To avoid potential issues due to scattering, the measurement device utilizes a spherical integrator which accounts for light which is refracted at different angles. The data for the loss of power by wavelength for AM 1.5 is shown in figure

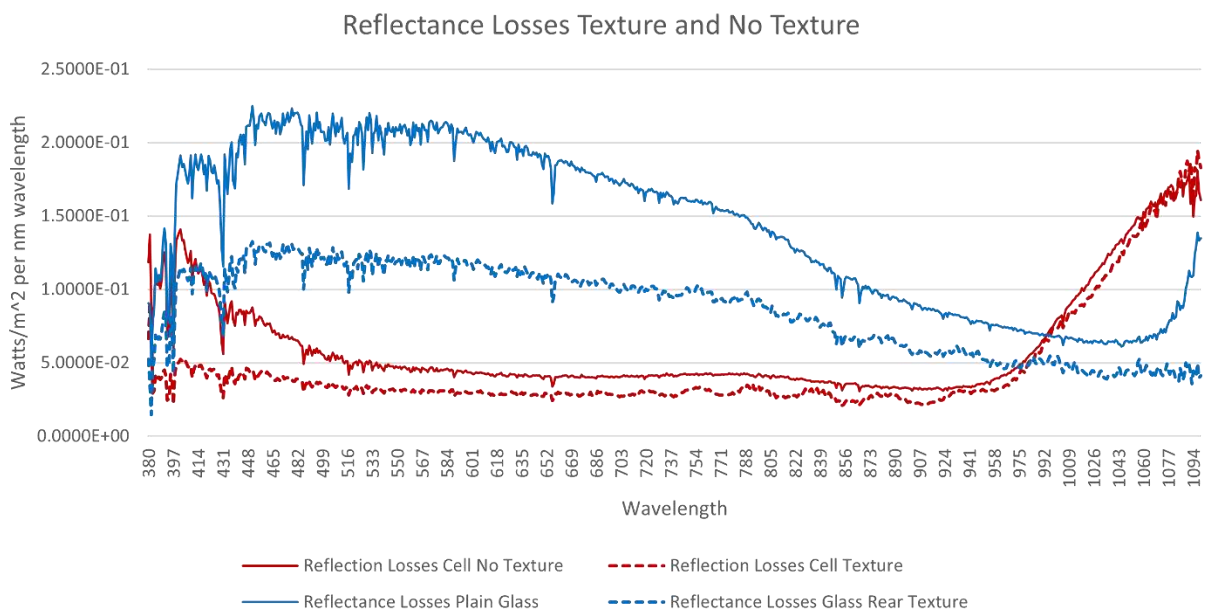


Figure 23: Measured reflection losses as a function of wavelength and adjusted to AM 1.5 incidence. Note that most of the gains are within the visible spectrum (380-700nm) especially when applied to the c-Si cell.

22.

The data is then put further analyzed utilizing quantum efficiency data for c-Si cells available in spreadsheet through collaboration with NREL (figure 23). While more energy can be emitted onto the cell itself, quantum efficiency by wavelength is also a key factor as the amount of energy which a PV

device is able to convert to energy is dependent on the number of electrons which may travel across the bandgap of the material and what the bandgap is. In other words, a single photon can only excite one electron (though there are some special materials such as quantum dots which can double the number of photons at certain wavelengths, that is significantly outside the scope of this thesis). First, AM 1.5 data is directly compared to data taken by members of the MEL of the local xenon lamp source as shown in section 2.3. Energy converted in excess of AM 1.5 on the xenon lamp is adjusted by wavelength and subtracted while energy converted which falls short of AM 1.5 is added. This is done by first taking the total energy and converting it to the spectral response. QE data is used in the following equation for each wavelength either in excess or which falls short:

$$SR = \frac{q\lambda}{hc} * QE \quad (2)$$

Where SR is the spectral response, q is the unit of elementary charge, h is Plank's constant, c is the speed of light, and QE is the quantum efficiency. However, this data is not yet corrected for the reflectance as the QE data taken from NREL is in terms of raw data. SR is then multiplied by $(1 - R)$ where R is the reflectance. This is done numerically over each wavelength and stored in a Microsoft Excel file. The equation for determining I_{sc} is:

$$I_{sc} = \int_{E_g}^{\infty} G(\lambda) * SR(\lambda) * (1 - R(\lambda)) * d(\lambda) \quad (3)$$

Where $G(\lambda)$ is the input irradiance and $SR(\lambda)$ is the spectral response. This is typically integrated from the bandgap energy, E_g , to infinity, however, the reflectance measurement device used was only effective from 400 to 1,100 nm or around 3 to 1.1 eV. Recall that rather than having to do the entire spectrum, a correction is needed instead. In the place of $G(\lambda)$ instead, energy in excess of AM 1.5 on the xenon lamp is used with a minus sign and energy which AM 1.5 is in excess of the Xenon lamp conditions

is given a plus sign. This allows for an accurate correction of the I_{SC} . Traditionally laminated cells are not corrected because the calibration device for xenon lamps is a traditionally laminated cell.

The total adjustment for improved current for AM 1.5 versus a xenon light source is found to be 1.5% relative correction when compared to reflection data for traditionally laminated cells. While this is

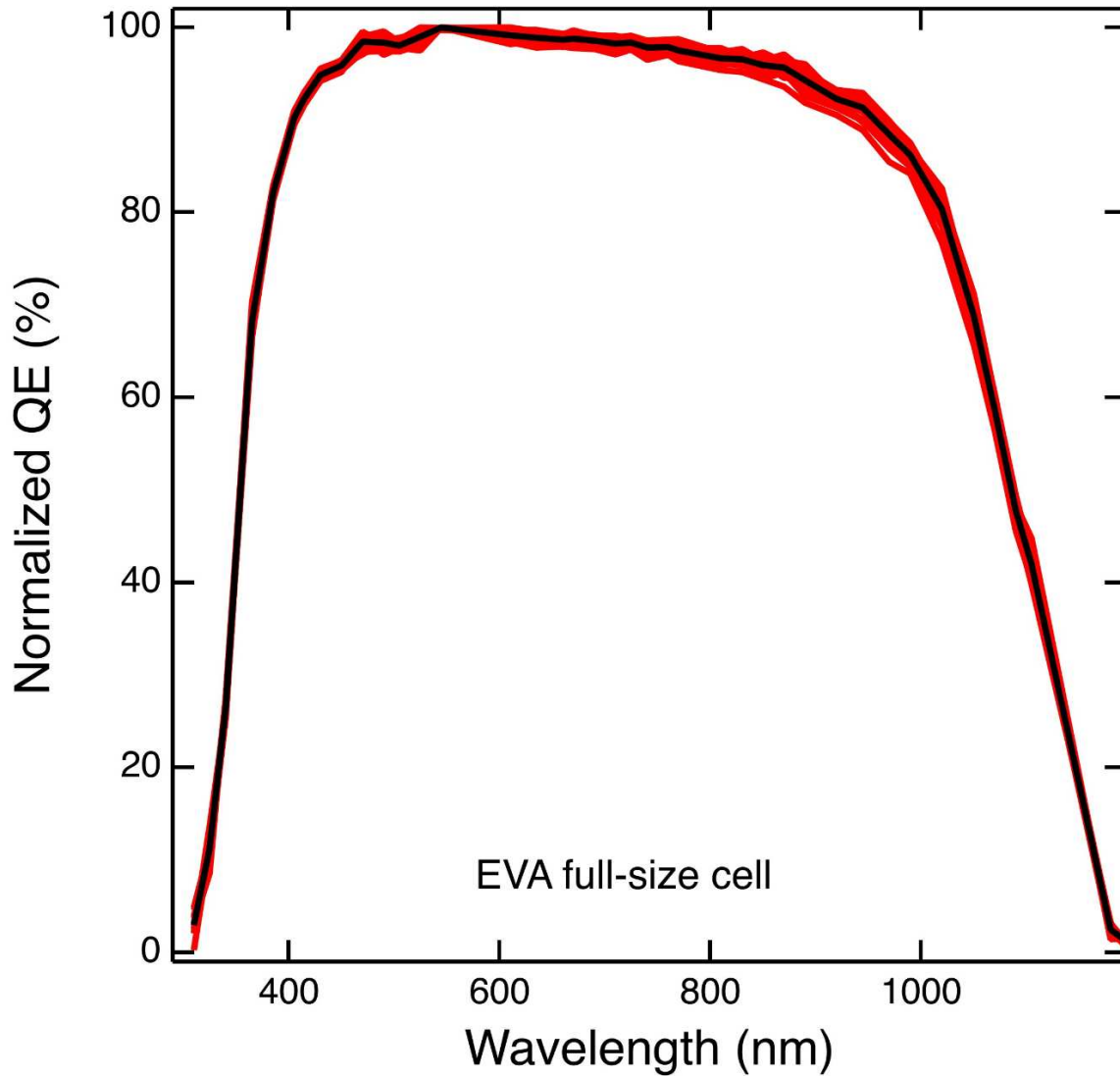


Figure 24: QE data as a function of wavelength normalized to number of incident photons courtesy of collaboration with NREL. Data is corrected for reflectance such that photons incident to the cell itself are considered.

significantly closer than results found by Apollon Solar where the correction for interior AR layers was much higher for adjusting for xenon lamp conditions as the reflectance of the texture is graphically flatter than AR layers, it does mean that when comparing varying module architectures, it is important to consider the light source of the measurement compared to the light source which will be generating power for the device, as well as the actual quantum efficiency of the solar cell itself.

Chapter 4: RESULTS AND DISCUSSION

4.1 Introduction

In this chapter, the results of each section will be shown and discussed. The overarching goal is to evaluate the data and what can be interpreted from the data. Each hypothesis is given its own section for the purpose of being able to discuss them individually within this chapter.

4.2 Hypothesis 1

The first hypothesis discussed earlier relates to bringing the leads through the sides of the module rather than the rear. This is primarily tested under damp heat conditions to pass a higher standard than is currently available. With the DOE goal of a 50-year lifespan for PV modules, this standard is the criteria for passing this hypothesis. Since bringing out the leads through the sides is less complex of a process, it also brings in a new challenge. While eliminating the rear junction box reduces one potential moisture breakthrough spot, it in fact introduces another. While eliminating a hole in the rear glass of the module also has significant benefits such as improved strength, the question of the effectiveness of an alternative is also important to ask. However, this may also be equally important for applications such as building integrated photovoltaics (BIPV) since these are intended to take the place of windows on sun-facing exterior walls of buildings. Leads which exit the side may be an important aesthetic choice. Rather than having wires which must be connected at the rear of these types of modules, the modules could be connected in series with minimal wires which may interfere with the light which enters the building.

For the first 3,000+ hours of testing, no significant visual change is noted in any of the modules. At 3,000 hours of testing, there is some discoloration in the sample which has leads protruding from the module but no onboard desiccant carrier for extra moisture absorption. At approximately 4,000 hours a

complete failure of all the moisture indicating strip has been observed (all moisture level indicators had turned pink). Results are tabulated in Table 2. The module with no leads exiting through the side and no onboard desiccant had completely passed 5,000 hours with no sign of moisture ingress. The module with leads exiting and onboard desiccant carrier had minor discoloration at the 5,000-hour mark but was not enough to show that a 10% humidity level had been reached on the interior of the module.

Table 2: Significant results from samples tested in DH conditions. Samples are removed from DH testing chamber every 1,000 hours and the moisture indicators are observed.

Module Description/Hours DH Testing	1,000	2,000	3,000	4,000	5,000
No leads exiting, no onboard desiccant carrier	No discoloration of moisture indicator	No discoloration of moisture indicator	No discoloration of moisture indicator	No discoloration of moisture indicator	No discoloration of moisture indicator
Leads exiting, no onboard desiccant carrier	No discoloration of moisture indicator	No discoloration of moisture indicator	Mild discoloration of moisture indicator	Significant discoloration of moisture indicator	Significant discoloration of moisture indicator
Leads exiting, onboard desiccant carrier	No discoloration of moisture indicator	No discoloration of moisture indicator	No discoloration of moisture indicator	No discoloration of moisture indicator	Mild discoloration of moisture indicator

indicate greater than 10% moisture internally. This is likely a sign that there was some moisture within the module at this point, but it was in fact lower than the 10% threshold to fully discolor the moisture indicator at the lowest humidity level the indicator could indicate.

These results are quite promising, as moisture internally when utilizing an iteration of the final design was intended to demonstrate potential for a 50-year lifespan in even the most humid climates. While the humidity indicated in the module with leads exiting and onboard desiccant carrier had taken in some moisture, internal desiccant load can be calculated to prevent failure of the module. The side junction box could also be reinforced against moisture ingress, however, there is no inherent benefit of having a rear junction box which also allows for moisture ingress. These results are quite promising as best optimized samples show significant robustness against moisture ingress, however, some design

improvements remain to be made. These improvements could potentially be considerate of the climate in the region for which the modules are to be deployed. For example, modules which are deployed in a high desert may not necessarily need as much internal desiccant as a module which is intended for use in a humid environment. This would allow cost savings where possible and increased protection for the module itself where necessary.

4.3 Hypothesis 2

The second hypothesis concerns the ability for the module to be disassembled easily enabling the recovery of high value recyclable materials. Recall that setting a time goal for this process should be equivalent to putting the module together. As discussed in section 3.2, there is some potential for issues to arise when completing tasks by hand and timing them. The data observed is fit to a decaying exponential. This is a somewhat sensible result since time and practice can yield significant improvements, however, it is important to find an optimal time which a machine could accomplish. This is accomplished using the equation below:

$$T_f = T_m e^{\frac{c}{n}} \quad (4)$$

Where T_f is the experimental time measured, n is the trial number, c is a fit constant, and T_m is the actual potential time it would take for manufacturing. This is because one might expect practice over time to reach some final time as the n term in $\frac{c}{n}$ goes to infinity. This leaves us with a predictable T_m for the process which is representative of a final expected manufacturing time.

Table 3: T_m for each process step

Process	Separation of Glass	Oscillating Multi-Tool Pass	Cleaning Tool Pass
Time for 60cm x 120cm samples	28 seconds	26 seconds	25 seconds

As can be seen here, the times are reduced to slightly below the manufacturing time which has been shown in other studies. This means that the process of disassembly for the encapsulation process is equivalent or equal to the time in which the module can be assembled even when accounting for movement to different process steps. With a 30 second cycle time, this can be adapted to large scale recycling processes which, due to the lack of vacuum lamination, are intrinsically easier to manage than traditional modules.

4.4 Hypothesis 3

The third hypothesis is that microcrack growth and formation can be significantly reduced to below detection limits due to lack of encapsulants. There is no growth of microcracks observed in best optimized samples. It is important to include data on overall performance of the module, however, the drop during A3 testing is not a good indicator of microcrack growth and formation unless it is encapsulated in EVA. This is because UV causes the EVA to increase in cross-link density which in turn hardens the material and can lead to the growth of microcracks. Instead, this was found to be a result of UV degradation specifically on the cell itself, likely due to boron dopants which are being replaced industry-wide for gallium dopants which do not experience the same degradation (Woodhouse, 2020).

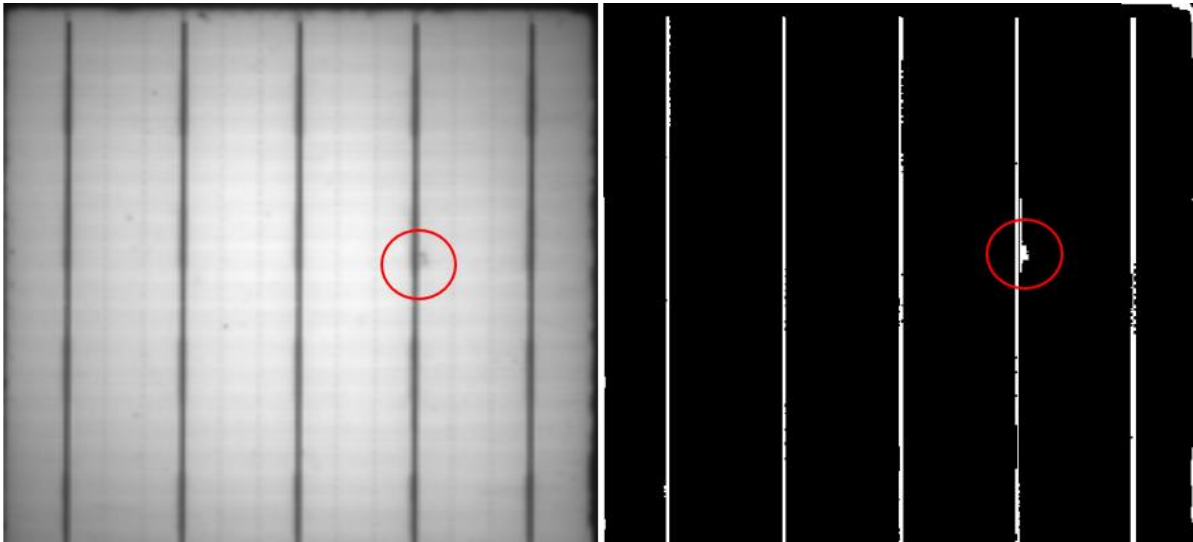


Figure 26: EL image pre and post processing utilizing Sobel edge detection methods. While the wires show up as not illuminating, it is more important to ask whether or not this grows. The circled image in the right shows the detection of an imperfection in the cell, however, it is not observed to have grown during accelerated stress testing.

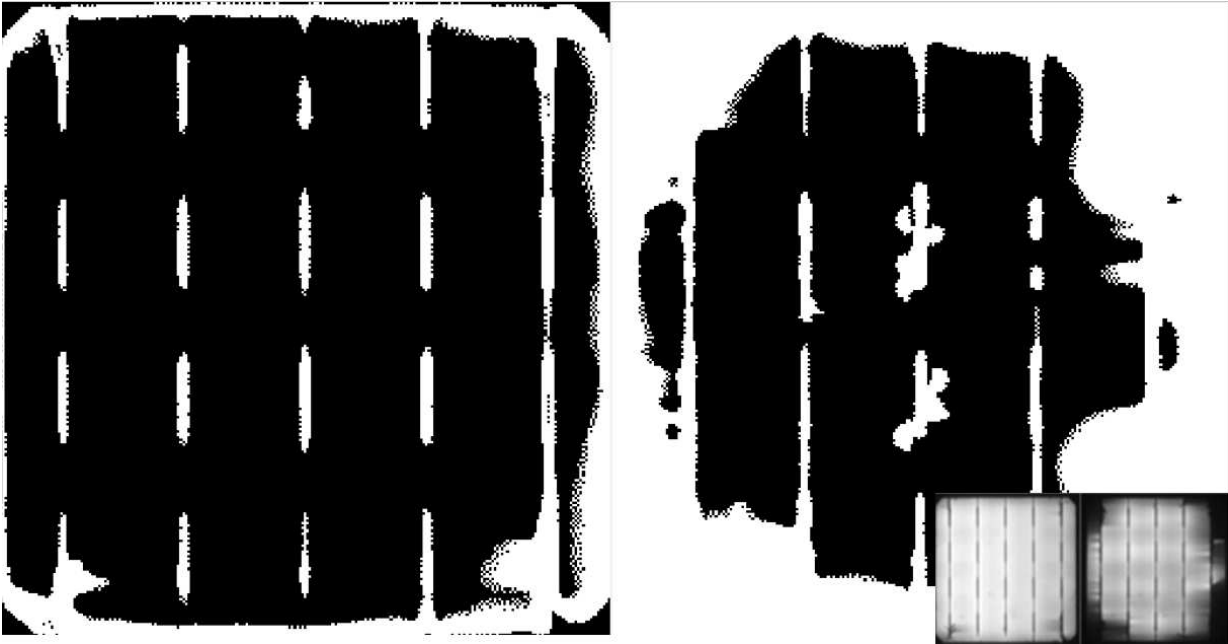


Figure 25: Glass-glass EVA module fabricated at NREL for comparison. Post-encapsulation (left) shows degradation due to extreme process conditions while post accelerated stress (right) demonstrates how microcracking can grow during stress tests.

When samples are best-optimized, there is no formation or growth of microcracks due to the encapsulation process. Though there are some observed, these are likely formed during the soldering

process which also has potential to damage the cell. Though somewhat rare in samples, even when cracks are present at the onset of production of a given sample, no significant differences can be seen between the EL or PL imaging before and after accelerated stress testing is shown in figure 16. When utilizing an image analysis program in MATLAB using region analysis which extracts statistical data with Sobel edge detection methods. That is that the affected areas are separated from the unaffected areas through large gradient changes from one pixel to the next. This is then divided into regions which are either not illuminating or illuminating. The difference between the percent of the cell which is illuminated versus not illuminated is measured before and after. However, any differences are within the margin of error of the measurement. The comparison is clear in many samples of modules that these microcracks become more likely due to the extreme process conditions of traditional lamination. These results are also compared to glass-glass modules which use EVA as an encapsulant since these have the most similar construction.

Table 4: Number of pixels detected which show low EL in cell. Because of the difficulty in getting the same exact image twice, there is significant error. However, there is little, or no change observed during accelerated stress testing so far.

Sample #	# Pixels Impacted Initial	# Pixels Impacted Final	Change Detected
ESM 5	1.5e3	1.4e3	No
ESM 6	1.3e3	1.1e3	No
ESM 7	2.5e3	2.6e3	No
ESM 8	2.9e3	3.0e3	No
Glass-Glass EVA (NREL)	8.2e3	31.5e3	Yes

No changes can be detected between the various cells before and after stress testing for ESM modules, however, several glass-glass EVA samples made show significant formation of microcracks both before and after encapsulation. This is because the image detection software is not as fine-tuned for

detecting changes when the changes are so insignificant, however, microcrack formation and growth can indeed be detected when it does occur. There is some error in the measurement as cells do not “improve” over time which is what has been measured. It should also be noted that samples 7 and 8 were both half-cut cells which creates a gap halfway between the cells. The total effected area, however, is not detected to be changing during repeated stress cycles. For example, the total area of the tabbing wires is also a significant factor but should not be considered in the onset or growth of microcracks.

4.5 Hypothesis 4

The fourth and final hypothesis is that current can be matched utilizing interior textures. Here the results of the most recent experiments are presented and discussed. As discussed, there are two primary experiments utilized to determine the ability to power match due to availability of testing equipment. One is a test under Xenon lamp conditions and the other is testing for reflectance losses in order to properly adjust the data for AM 1.5 spectrum light. The numerical integration of the reflectance data which subtracts the performance where incident light such as IR is in excess of AM 1.5 under xenon conditions and addition of performance such as under visible light where the Xenon lamp outputs less than AM 1.5 is conducted and approximated to yield a relative increase of 1.5% current for the non-vacuum lamination architecture. Data for each measurement is taken and plotted in figure 26.

When the data is properly adjusted for AM 1.5, there is no statistically significant performance difference

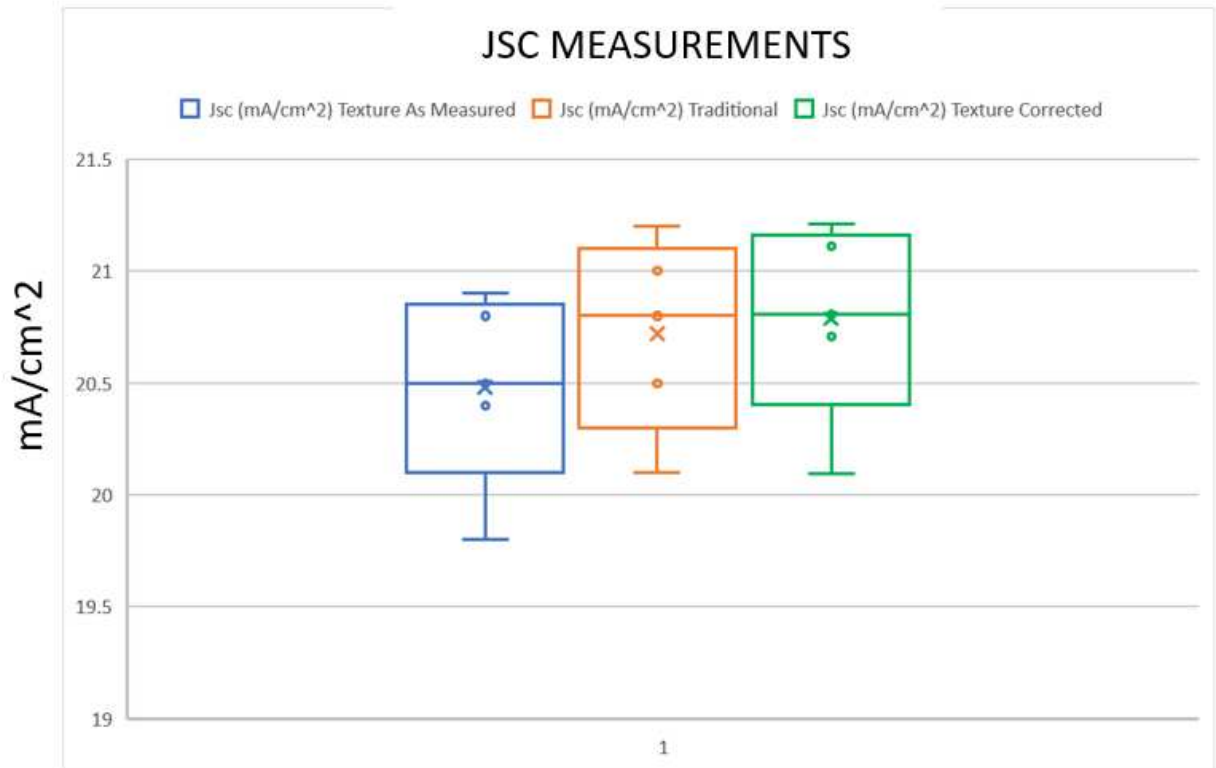


Figure 26: Current density (J_{sc}) as measured under xenon lamp conditions for ESM under, J_{sc} for traditional lamination under xenon lamp, and J_{sc} for ESM adjusted for AM 1.5 based on reflectance data.

between traditional lamination and the module architecture being researched at MEL. One additional consideration is that the texture could potentially be continuously improved, however, based on the lack of UV absorption in the simulated module architecture due to replacing the EVA with a clear silicone gel, this is an even more significant result. As discussed in section 4.3, the need for some UV blocking properties may be necessary to prevent degradation of the cells due to UV or, in the case of improved cell reliability, it may be necessary to match power with traditional modules without the use of any UV blocker since EVA is currently being adapted to increase the transmittance of UV light in order to attain higher module performance as UV makes up approximately 2% of the AM 1.5 spectrum (Voght et al., 2016).

Chapter 5: CONCLUSIONS

5.1 Conclusions

After a significant number of tests, this research serves as a significant step forward in proof-of-concept for ESM architecture. The lack of encapsulation represents a significant cost savings in terms of module production, but with potential for improved reliability and performance matching capabilities of traditional module architectures this then becomes a more viable solution. While nothing can be declared without absolute certainty, it is important to note that the findings of this work represent a significant progress step towards creating a viable alternative to traditional encapsulation methods. The general status of the hypothesis is listed below:

- Design simplification for bringing the leads from the sides has been shown to be possible while retaining 5,000-hour resistance against damp heat or 50-year lifespan in a humid climate such as Bangkok or Miami.
- The recovery of valuable materials is shown possible through disassembly of the module in process times which can be attained at equal to or less than the assembly time.
- Microcrack formation and growth is shown to be eliminated below detection limits due to the lack of traditional lamination processes and stresses.
- ESM samples are capable of power matching when compared to identical cells which are traditionally encapsulated.

The first significant finding is that this module architecture not only passes the minimum requirements outlined in IEC 61215 for DH testing but is able to surpass them by a factor of 5 or more by simply adding more desiccant carrier. This can be utilized in the module architecture as both support and

The other factor is the reduction in cost in recovery of valuable materials. C-Si PV modules utilize silver, copper, and high-purity Si, which can all be recovered once the encapsulation is removed. By demonstrating a time for processing which can match the time of production for encapsulation, this process may have significant economic benefit as materials become more difficult to mine and mining practices become more intensive and more impactful to the environment.

The reduction of microcrack formation and growth has been somewhat significant. This is somewhat intuitive since mechanical stresses are greatly reduced for ESM compared to the vacuum

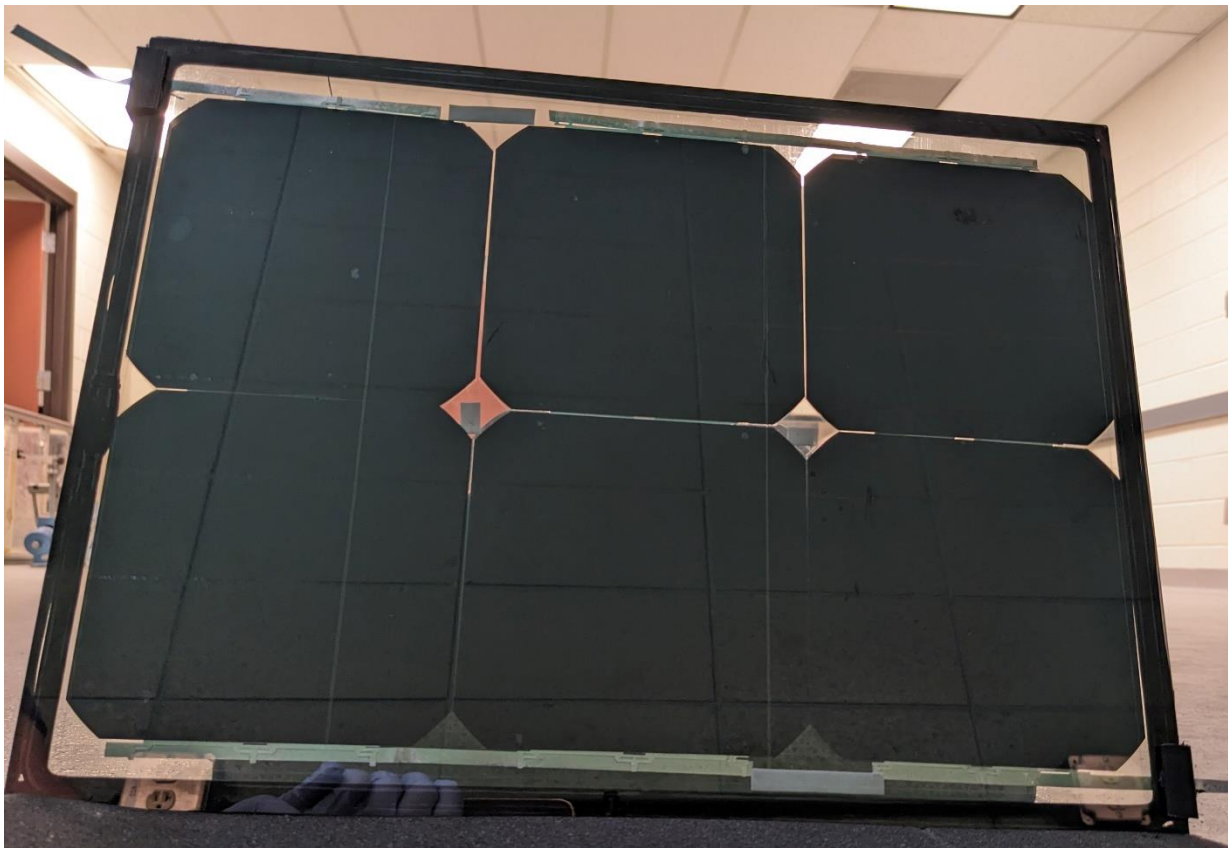


Figure 27: 20cm x 30cm 6 cell 20-watt prototype module fabricated at MEL. This is the most recent and most powerful module created by the multitude of processes developed at MEL for c-Si to date. Cells are of a configuration which is also extremely resilient against UV degradation.

lamination process.

Finally, larger, and fully functioning prototypes of this module architecture should be fabricated such as the example shown in figure 27. This will involve cell selection, further design, and process optimization, as well as custom and specialty tools for improving the manufacturing process. Significant work towards this has already been done and will continue for the near future as this technology moves towards production.

5.2 Future work and recommendations

While there has been a significant amount of progress, there is still continued work to be done in terms of developing this technology. This means primarily ensuring that full-size modules can meet or exceed current or potential future standards in PV technology.

Continued extended (5,000 hour) DH testing with circuit plates to measure performance. Devices such as CdTe and perovskites may be a better indicator of moisture ingress than the 10% indicating samples with indicators at increments of 10% at each step as this introduces significant error. This work may provide better insight into actual internal moisture levels and give a more precise indicator of acceleration factors while also showing more accurately if moisture has in fact impacted the performance of the module.

Accelerated testing should be continued at NREL. This test structure should be repeated multiple times and in accordance with industry standards. This will be a better indication of a more complete resistance to microcrack formation and growth since this can be somewhat more intense than only thermal cycling. Samples should also be exposed to hail impact as well as mechanical stress and strain.

Removal of nanostructure has also been demonstrated in more recent experiments. Cost analysis of the entire process would be a key finding. The nanostructure material is easily removed in a bath of MEK. While this may be a lengthier step but could be done with a significant number of cells in

parallel with relatively small space. Understanding the total cost of the entire process through techno-economic assessment is a good goal moving forward.

Microcrack growth and formation needs further testing still with nanostructure applied to include A3 testing. This adds a new layer of complexity, however, the ability of the material to expand within the module is likely a significant improvement (including the reduced process temperatures). This should include every test being repeated with a statistically significant number of samples through an independent organization such as NREL.

REFERENCES

1. Ahsan, S.M. and Khan, H.A. (2019), Performance comparison of CdTe thin film modules with c-Si modules under low irradiance. *IET Renewable Power Generation*, 13: 1920-1926. <https://doi.org/10.1049/iet-rpg.2018.5479>
2. Amine Allouhi, Shafiqur Rehman, Mahmut Sami Buker, Zafar Said, Up-to-date literature review on Solar PV systems: Technology progress, market status and R&D, *Journal of Cleaner Production*, Volume 362, 2022, 132339, ISSN 0959-6526, <https://doi.org/10.1016/j.jclepro.2022.132339>.
3. Barretta, C., Oreski, G., Feldbacher, S., Resch-Fauster, K., Pantani, R. (2021). Comparison of Degradation Behavior of Newly Developed Encapsulation Materials for Photovoltaic Applications under Different Artificial Ageing Tests. *Polymers*, 13(2), 271. <https://doi.org/10.3390/polym13020271>
4. Barth, K., Morgante, J., Sampath, W. S., Shimpi, T., & Maple, L. (2018). Advanced Encapsulation Technology for Reduced Costs, High Durability and Significantly Improved Manufacturability. *IEEE PVSC 2018*. <https://doi.org/10.1109/pvsc.2018.8548213>
5. Barth, K., "Abound Solar's CdTe module manufacturing and product introduction," *2009 34th IEEE Photovoltaic Specialists Conference (PVSC)*, Philadelphia, PA, USA, 2009, pp. 002264-002268, doi: 10.1109/PVSC.2009.5411358.
6. Couderc, R., Amara, M., Degoulange, J., Madon, F., & Einhaus, R. (2017). Encapsulant for glass-GLASS PV modules for minimum optical losses: Gas or Eva? *Energy Procedia*, 124, 470–477. <https://doi.org/10.1016/j.egypro.2017.09.283>
7. Deng, R., Chang, N. L., Ouyang, Z., amp; Chong, C. M. (2019). A techno-economic review of silicon photovoltaic module recycling. *Renewable and Sustainable Energy Reviews*, 109, 532–550. <https://doi.org/10.1016/j.rser.2019.04.020>
8. Dupuis, J., Saint-Sernin, E., Nichiporuk, O., Lefillastre, P., Bussery, D., & Einhaus, R. (2012). NICE module technology - From the concept to mass production: A 10 years review. *2011 36th IEEE Photovoltaic Specialists Conference (PVSC)*, Seattle, WA, USA, 2009, <https://doi.org/10.1109/pvsc.2012.6318254>
9. Ellis, S., Maple, L., Shimpi, T., TamizhMani, G., Sampath, W. S., Pavgi, A., & Barth, K. (2020). Demonstration of Non-Lamination Encapsulation Techniques for Thin Film Solar Modules. *IEEE PVSC 2020*. <https://doi.org/10.1109/pvsc45281.2020.9300665>
10. Green, M. Commercial progress and challenges for photovoltaics. *Nat Energy* 1, 15015 (2016). <https://doi.org/10.1038/nenergy.2015.15>
11. Handara, V., Radchenko, I., Tippabhotla, S. K., Narayanan, K. R., Illya, G., Kunz, M., Tamura, N., & Budiman, A. S. (2017). Probing stress and fracture mechanism in encapsulated thin silicon solar cells by synchrotron X-ray microdiffraction. *Solar Energy Materials and Solar Cells*, 162, 30–40. <https://doi.org/10.1016/j.solmat.2016.12.028>
12. Horowitz, Kelsey, Et. Al. A Techno-Economic Analysis and Cost Reduction Roadmap for III-V Solar Cells, NREL, 2018.
13. Jones-Albertus, R., Feldman, D., Fu, R., Horowitz, K., & Woodhouse, M. (2016). Technology advances needed for photovoltaics to achieve widespread grid price parity. *Progress in Photovoltaics: Research and Applications*, 24(9), 1272–1283. <https://doi.org/10.1002/pip.2755>
14. Kempe, M. D., Dameron, A. A., & Reese, M. O. (2013). Evaluation of moisture ingress from the perimeter of photovoltaic modules. *Progress in Photovoltaics: Research and Applications*, 22(11), 1159–1171. <https://doi.org/10.1002/pip.2374>
15. Kempe, M., Watts, A., Shimpi, T., Ellis, S., & Barth, K. (2023). Modeling of the effectiveness of novel edge seal designs for fast, low-Cap-Ex manufacturing. *Energy Science & Engineering*, 11(7), 2314–2329. <https://doi.org/10.1002/ese3.1455>

16. Kontges, M., Kurtz, S., Berger, K. A., & Jahn, U. (2014). Review of Failures of Photovoltaic Modules. INTERNATIONAL ENERGY AGENCY PHOTOVOLTAIC POWER SYSTEMS PROGRAMME. <https://doi.org/978-3-906042-16-9>
17. Mittag, M., Eitner, U., & Neff, T. (2017). TPEDGE: Progress on Cost-Efficient and Durable Edge-Sealed PV modules. *European PV Solar Energy Conference and Exhibition*, 33.
18. Pacca, Sergio, S. Deepak, and G.A. Keoleian. 2005. Life Cycle Assessment of the Photovoltaic System in Dana Building: Thin Film Laminates, Multi-crystalline Modules and Balance of System Components. University of Michigan: Ann Arbor: 1-106
19. Ruhle, R., DeLazzer, T., Johnston, S., Kern, D., & Sampath, W. (2023). Novel Module Architecture for Lower Capex And Improved Recyclability For C-Si Pv Modules. *Proceedings of the 2023 PVSC-50* [Manuscript in preparation].
20. Song, W., Tippabhotla, S. K., Tay, A., & Budiman, A. S. (2018). Numerical simulation of the evolution of stress in solar cells during the entire manufacturing cycle of a conventional silicon wafer based photovoltaic laminate. *IEEE Journal of Photovoltaics*, 8(1), 210–217. <https://doi.org/10.1109/jphotov.2017.2775158>
21. Shimpi, T., Moffett, C., Sampath, W. S., & Barth, K. (2019). Materials selection investigation for thin film photovoltaic module encapsulation. *Solar Energy*, 187, 226–232. <https://doi.org/10.1016/j.solener.2019.04.095>
22. Tippabhotla, S. K., Song, W., Tay, A. A., & Budiman, A. (2019). Effect of encapsulants on the thermomechanical residual stress in the back-contact silicon solar cells of photovoltaic modules – A constrained local curvature model. *Solar Energy*, 182, 134–147. <https://doi.org/10.1016/j.solener.2019.02.028>
23. Vogt, M. R., Holst, H., Schulte-Huxel, H., Blankemeyer, S., Witteck, R., Hinken, D., Winter, M., Min, B., Schinke, C., Ahrens, I., Köntges, M., Bothe, K., & Brendel, R. (2016). Optical Constants of UV Transparent EVA and the Impact on the PV Module Output Power under Realistic Irradiation. *Energy Procedia*, 92, 523–530. <https://doi.org/10.1016/j.egypro.2016.07.136>
24. Wirth, H., Eitner, U., Hoffmann, S., Neff, T., Haedrich, I., & Mittag, M. (2015b). TPEDGE: Qualification of a Gas-Filled, Encapsulation-Free Glass-Glass photovoltaic module. *31st European Photovoltaic Solar Energy Conference and Exhibition*, 93–99. <https://doi.org/10.4229/eupvsec20152015-1co.11.4>
25. Wiser, Ryan H., Bolinger, Mark, & Seel, Joachim. *Benchmarking Utility-Scale PV Operational Expenses and Project Lifetimes: Results from a Survey of U.S. Solar Industry Professionals*. United States. <https://doi.org/10.2172/1631678>
26. Wisniewski, D, Lv, R, Nair, SV, Jaubert, J-N, Xu, T, Ruda, HE. Measurement and modelling of water ingress into double-glass photovoltaic modules. *Prog Photovolt Res Appl*. 2019; 27: 144–151. <https://doi.org/10.1002/pip.3069>
27. Woodhouse, Michael, Repins, Ingrid, & Miller, David. *LID and LeTID Impacts to PV Module Performance and System Economics: Draft Analysis*. United States.

APPENDIX A- PUBLICATIONS

1. NREL 2023 PVRW poster presentation “Novel Module Architecture for Improved Recovery of High-Value Recycling and Streamlined Approach to Encapsulation to Lower Manufacturing Cost and Improved Reliability”
2. Ruhle, R., DeLazzer, T., Johnston, S., Kern, D., & Sampath, W. (2023). Novel Module Architecture for Lower Capex And Improved Recyclability For C-Si Pv Modules. *Proceedings of the 2023 PVSC-50* [Manuscript in preparation]. -Also Nominated for Best Poster Award